New Astronomy Reviews 92 (2021) 101610

Contents lists available at ScienceDirect

New Astronomy Reviews

journal homepage: www.elsevier.com/locate/newastrev

Numerical simulations of jets

Serguei Komissarov [a], Oliver Porth [b,*]

[a] Department of Applied Mathematics, University of Leeds, Leeds LS2 9JT, UK
[b] Anton Pannekoek Institute for Astronomy, University of Amsterdam, Science Park 904, 1098 XH, Amsterdam, The Netherlands

ARTICLE INFO

Keywords:
Instabilities
MHD
Relativistic processes
Methods: Numerical
Galaxies: Jets

ABSTRACT

When astrophysical jets were discovered one hundred years ago, the field of numerical simulations did not yet exit. Since the arrival of programmable computers though, numerical simulations have increasingly become an indispensable tool for dealing with "tough nut" problems which involve complex dynamic and non-linear phenomena. Astrophysical jets are an ideal example of such a tough nut, where multi-scale plasma physics, radiative and non-thermal processes, turbulence and relativity combine to present a formidable challenge to researchers.

Highlighting major achievements obtained through numerical simulations concerning the validity and nature of the Blandford–Znajek mechanism, the launching, collimation, acceleration and stability of jets, their interaction with the surrounding plasma, jet-galaxy feedback mechanisms etc., we trace how the field developed from its first tentative steps into the age of "maturity". We also give a brief and personal outlook on how the field may evolve in the foreseeable future.

1. Introduction

1.1. The numerical approach

Twenty five years after the discovery of the M87 jet by Curtis (1918), the efforts of the British to break encrypted communications of the Germans during the WW2 were facilitated by the arrival of the first ever electronic programmable computer Colossus (Copeland, 2006). Two years later, US military was provided with ENIAC, the first "Turing-complete" or "computationally-universal" electronic computer (Copeland, 2017). These ancestors of modern computers were huge, cumbersome, slow and had very limited memory, but they paved the way to the technological revolution which affected all aspects of modern society, including science.

In theoretical physics, natural phenomena are described by various mathematical equations. Some of them are purely descriptive, like the equations of the particle kinematics. But the most important ones only formulate the laws that govern the evolution of physical systems. As such they do not just provide ready-made descriptions to any particular process or phenomena. Instead such specific descriptions have to be found via solving these dynamic equations given the conditions of the specific problem under consideration. These dynamical laws are ordinary or partial differential equations.

On rare occasions, exact solutions can be found in the form of well-studied analytic functions or infinite expansions in terms of such functions. Normally, this is the case where the dynamical laws are linear equations. Unfortunately for the theorists, most natural phenomena are more complex than this and governed by non-linear equations. This causes theorists to take the route of simplification. For example, a number of terms in the equations can be ignored. A number of symmetry conditions on the types of solutions can be imposed, allowing to reduce the dimensionality of the problem and hence deal with dynamic laws of simpler form. Quite often these conditions are rather artificial and driven not as much by the nature of the physical phenomena under consideration but rather by the desire to deal with an analytically-tractable mathematical problem. Finally, one may consider problems which involve small parameters or deal only with asymptotic regimes and look for approximate analytic solutions. Quite often the complexity comes from the large number of interacting components. For example, in Newtonian mechanics, the problem of motion under the action of gravity has a general analytic solution in the case of two interacting point bodies (masses), but already in the case of three bodies a general solution does not exist. Similarly, the dynamics of a system of microscopic particles interacting electromagnetically (plasma) can only be studied numerically. The fluid model of plasma simplifies the problem and yet the number of interacting components in this model is formally infinite since the fluid systems are continuous in space.

As an alternative to the analytic approach, one can look for a numerical representation of solutions. For example, the space–time

* Corresponding author.
E-mail address: o.porth@uva.nl (O. Porth).

https://doi.org/10.1016/j.newar.2021.101610
Received 23 September 2020; Accepted 9 January 2021
Available online 23 January 2021
1387-6473/

domain of a fluid model can be covered by a grid of points and in every point of the grid the fluid can described by the local values of its dependent variables. In order to represent the solution, the values at the neighboring points have to satisfy the approximate discrete versions of the governing differential equations. In this way, an infinite number of interacting elements is replaced with a finite number. Obviously, for the numerical solution to be reasonably accurate the number of grid points has to be large and so is the amount of calculations needed to populate them with the values of dependent variables. This is why before the arrival of powerful computers, the numerical approach was practical only for a rather limited number of mathematical problems.

Since 1960 the computational power of the most powerful supercomputer in the world was doubling on average every 18 months and has increased by the whooping 10^{12} times. Miniaturization of computer chips, ever decreasing cost of their manufacturing, development of high-speed networks and software for distributed computing are behind this rapid advance. The design of supercomputers has changed from single units to compute clusters. The power of second-tier supercomputers has been growing at similar rate and what yesterday could be afforded only by the big national research centers of rich countries is available today at many research institutes and research-active universities.

This technological revolution has changed dramatically the role of the numerical approach and moved it from the periphery of scientific exploration to the very center of modern research. Whereas in the past it could be used to deal only with rather limited types of problems, nowadays it allows to simulate the dynamics of complex natural phenomena. A new branch of theoretical research has emerged, which can be described as experimental theoretical science. It is based on creating a kind of artificial reality and carrying out controlled experiments aimed at learning more about nature. Provided the theoretical framework (the set of evolution equations) is adequate, the numerical method is efficient and the computational power is sufficient, the outcome can be very close to reality in many respects. This approach is particularly valuable where real experiments are practically impossible, which includes the whole of Astrophysics.

1.2. Astrophysical jet plasma

The astrophysical jets are high-velocity flows of plasma/gas. Although this plasma is very rarefied and often collisionless, there are good reasons to believe that the fluid description of the jet dynamics is mostly adequate (Begelman et al., 1984). The Larmor gyration and collective interactions are expected to introduce an effective collisional free path which is much smaller compared to the free path for the two-body Coulomb interaction. The same applies to many other astrophysical phenomena. For this reason, the efforts of astrophysical numericists have been focused on developing of efficient computational tools for compressible fluid dynamics and magnetohydrodynamics. For future reference, here we present the Newtonian and relativistic versions of these system of equations written in the form of conservation laws.

Ideal compressible Newtonian hydrodynamics (HD) includes the conservation laws for the mass

$$\partial_t \rho + \nabla\cdot(\rho\mathbf{v}) = 0\,, \tag{1}$$

energy

$$\partial_t(\rho v^2/2 + e) + \nabla\cdot((\rho v^2/2 + w)\mathbf{v}) = 0\,, \tag{2}$$

and momentum

$$\partial_t \rho\mathbf{v} + \nabla\cdot(\rho\mathbf{v}\mathbf{v} + p\mathbf{g}) = 0\,, \tag{3}$$

where ρ, p, e, $w = e + p$ and $\mathbf{v}$ are the mass density, pressure, thermal energy, enthalpy and velocity of the fluid respectively and $\mathbf{g}$ is the metric tensor of Euclidean space. Source terms may replace the zeros on the right-hand side of these equations when gravity, radiation, mass-loading etc. are dynamically important. To close the system we need additional equations which express the relationships between the thermodynamic parameters, the so-called equation of state (EoS).

The corresponding laws of ideal special relativistic hydrodynamics (SRHD) are

$$\partial_t \rho\gamma + \nabla\cdot(\rho\gamma\mathbf{v}) = 0\,, \tag{4}$$

$$\partial_t(w\gamma^2 - p) + \nabla\cdot(w\gamma^2\mathbf{v}) = 0\,, \tag{5}$$

and momentum

$$\partial_t w\gamma^2\mathbf{v} + \nabla\cdot(w\gamma^2\mathbf{v}\mathbf{v} + pc^2\mathbf{g}) = 0\,, \tag{6}$$

where $w = \rho c^2 + e + p$ is the relativistic enthalpy which includes the rest mass-energy density of plasma particles and $\gamma = (1 - v^2/c^2)^{-1/2}$ is the Lorentz factor with the speed of light c. All the thermodynamic parameters are defined as measured in the reference frame comoving with the fluid.

The conservation laws of perfect Newtonian magnetohydrodynamics (MHD) are

$$\partial_t \rho + \nabla\cdot(\rho\mathbf{v}) = 0\,, \tag{7}$$

$$\partial_t(\rho v^2/2 + e + B^2/8\pi) + \nabla\cdot((\rho v^2/2 + w + B^2/4\pi)\mathbf{v} - (\mathbf{v}\cdot\mathbf{B})\mathbf{B}) = 0 \tag{8}$$

and

$$\partial_t \rho\mathbf{v} + \nabla\cdot(\rho\mathbf{v}\mathbf{v} - \mathbf{B}\mathbf{B}/4\pi + (p + B^2/8\pi)\mathbf{g}) = 0\,. \tag{9}$$

In addition the system includes the Faraday law

$$\frac{1}{c}\partial_t\mathbf{B} + \boldsymbol{\nabla}\times\mathbf{E} = 0\,, \tag{10}$$

the Gauss law

$$\nabla\cdot\mathbf{B} = 0 \tag{11}$$

and the perfect conductivity equation

$$\mathbf{E} = -\frac{1}{c}\mathbf{v}\times\mathbf{B}\,. \tag{12}$$

The Faraday equation can also be treated as a conservation law. Only the magnetic field $\mathbf{B}$ contributes to the electromagnetic energy density and pressure, as the electric field is small for $v \ll c$. Although we retained c in (10) and (12), it cancels out upon the substitution of $\mathbf{E}$ (12) into (10).

The conservation laws of ideal special relativistic magnetohydrodynamics (SRMHD) are

$$\partial_t \rho\gamma + \nabla\cdot(\rho\gamma\mathbf{v}) = 0\,, \tag{13}$$

$$\partial_t(w\gamma^2 v^2/2 - p + e_m) + \nabla\cdot(w\gamma^2\mathbf{v} + \mathbf{S}) = 0\,, \tag{14}$$

$$\partial_t(w\gamma^2\mathbf{v} + \mathbf{S}) + \nabla\cdot(w\gamma^2\mathbf{v}\mathbf{v} - (\mathbf{E}\mathbf{E} + \mathbf{B}\mathbf{B})c^2/4\pi + (p + p_m)c^2\mathbf{g}) = 0\,, \tag{15}$$

where $p_m = (B^2 + E^2)/8\pi$ is the electromagnetic pressure $e_m = p_m$ is the electromagnetic energy density, and $\mathbf{S} = (\mathbf{E}\times\mathbf{B})c/4\pi$ is the Poynting flux. The Faraday law, the Gauss law and the perfect conductivity condition are exactly the same as in the Newtonian MHD. Here $\mathbf{B}$, $\mathbf{E}$ are the magnetic and electric fields as measured in the frame where the fluid is moving with the velocity $\mathbf{v}$, the so-called laboratory frame.

The inclusion of general relativistic effects does not fundamentally alter the nature of the equations for the magnetohydrodynamical (test-) fluid (Anile and Pennisi, 1987). Especially when written in terms of the physical parameters as measured by a local fiducial observer at rest in the space of a 3+1 spacetime splitting, the general relativistic versions of HD and MHD take on a form very similar to the special relativistic variant (e.g. Koide, 2003; Del Zanna et al., 2007). In essence, the equations remain hyperbolic conservation laws where gravity enters through source terms (e.g. Komissarov, 1999a, 2001b, 2004b; Porth et al., 2017).

The most successful approach for these systems is based on the so-called upwind numerical schemes for hyperbolic systems of conservation laws. This approach allows to preserve the global integrals of motion, such as the total energy, mass and momentum down to the rounding error of computer processors and handle shock waves very accurately even in the simulations with rather low grid resolution (e.g. Martí and Müller, 2015). Magnetohydrodynamics presents an additional challenge as the magnetic field must satisfy the Gauss law. Although this differential constraint is preserved by the exact Faraday equation, this is not necessarily true for its discretized versions, which may lead to large errors and even to complete corruption of the numerical solution. A number of successful techniques has been developed to deal with this issue, such as the constraint transport (CT) (Balsara and Spicer, 1999; Evans and Hawley, 1988) and generalized Lagrange multiplier (GLM) methods (Dedner et al., 2002). Another important advance is the development of adaptive grid techniques, which allows to increase the numerical resolution in highly dynamic regions with interesting small-scale structures and reduce it elsewhere. Finally, the development of publicly available codes has allowed a much broader astrophysical community with less advanced coding skills to carry out computer simulations.

2. Infancy

The first numerical study of astrophysical jets was carried out by Rayburn (1977). They focused on the structure created via the interaction of a 2D uniform supersonic cylindrical non-relativistic and unmagnetized flow with an external medium of either uniform density or density decreasing with the distance from the injection nozzle. They used a particle-in-cell code (PIC) for fluid dynamics where the fluid is represented by a collection of macro-particles. The computational grid had just 10×20 grid cells and 16 particles per cell. Yet, they were able to confirm the development of two shocks — the forward bow shock driven by the jet into the external gas and the reverse shock terminating the supersonic flow of the jet itself (Scheuer, 1974; Blandford and Rees, 1974). They also observed the development of a rarefied cocoon around the jet made out of gas heated at the termination shock, see Fig. 1 of a reproduction from the paper by Rayburn (1977).

Norman et al. (1981) used non-relativistic 2D hydro-simulations to see if a hot gas continuously supplied in the center of a gravitationally bound cloud can escape in the form of jets as this was envisaged in the twin-exhaust model (Blandford and Rees, 1974). They used a finite difference code on a 40×40 grid. The results of the simulations did not quite agree with the theoretical model. The hot gas did form a cavity inside the cloud but did not uniformly fill it like in the combustion chamber of a rocket engine. Instead, it produced a supersonic wind emerging from its source and terminating at a spherical shock. Only after this the hot shocked gas escaped along the least resistance route through the channel shaped in the form of the Laval nozzle. Moreover, the central cavity developed the Rayleigh–Tailor instability capable of destroying the nozzle. This was a very good early example of how computer simulations can be used to develop a much better understanding of an astrophysical problem compared to a highly simplified and over-constrained theoretical model. The history of jet studies has many examples like this.

Later, a similar approach was used by MacFadyen and Woosley (1999) and Aloy et al. (2000) in their study of the possibility to generate jets during the gravitational collapse of massive rotating stars, with application to GRBs. In these 2D Newtonian simulations a large amount of energy was continuously deposited in the polar region above the hyper-accreting disk which was cooling via neutrino emission. The rate of the energy deposition was based on the estimated annihilation rate of the disk-emitted neutrinos. Initially, the inertia of the gas accreting via the polar region was too great to overcome but in time, the supply of low angular momentum mass reduced, the density in the polar region dropped and powerful supersonic jets emerged from the energy deposition region. These jets were collimated by the centrifugally-supported "walls" of the accreting gas.

Norman et al. (1982) carried out the first systematic study of non-relativistic axisymmetric fluid jets drilling their way through a uniform external gas. The setup was similar to that of Rayburn (1977) but with much higher numerical resolution, 240×60 grid, and a different numerical approach. The simulations were carried out on a CRAY-1 supercomputer with each run requiring 2–3 h of CPU time. They not only confirmed the large scale structure found in Rayburn's study but also revealed a lot of new fine details, including the quasi-stationary chain of conical shocks driven into the jet by the high pressure of its cocoon, the development of the Kelvin–Helmholtz instability and mixing at the jet/cocoon interface and the interface separating the shocked external gas from the shocked jet gas in the cocoon. In the setup, the density ρ_e and pressure p_e of the external gas were fixed and the jet pressure at the inlet was assumed to be the same as that of the external gas, $p_j = p_e$. The numerical models were differentiated by the density ratio $\eta = \rho_j/\rho_e$ and the jet Mach number $M_j = v_j/a_{s,j}$ at the inlet ($a_{s,j}$ is the jet sound speed.). Obviously, higher values of η and M_j imply a higher jet thrust and hence a higher advance speed of its head v_h and only when $v_h \ll v_j$ the jet is expected to inflate an extensive cocoon. This expectation was confirmed and quantified in the simulations.

In the jet simulations by Rayburn (1977) and Norman et al. (1982), as well as in the numerous other studies that followed, the jets were injected into the computational domain as cylindrical flows with velocities perfectly aligned to the symmetry axis. Such a perfect collimation ignores the initial expansion of astrophysical jets on their way from the central engine to the remote locations where the observed interaction with the external gas takes place. This expansion can be inhibited when the external pressure becomes sufficiently large to bend the jet streamlines and thus increase its collimation. In supersonic jets this must be achieved via a conical shock wave called a collimation or reconfinement shock. The steady-state structure of supersonic jets reconfined by the pressure of hot coronas of giant elliptical galaxies was first studied by Sanders (Sanders, 1983), who used the method of characteristics, and then by Falle and Wilson (1985), who used time-dependent simulations accelerated via a multigrid technique. In the latter study the finest grid had 144×2192 cells allowing more than 24 cells per jet radius. The studies have shown that the recollimation shock triggers a downstream chain of conical shocks with progressively increasing separation between them which was reminiscent of the chain of bright knots in the M87 jet. Fig. 2 illustrates the sequence of reconfinement shocks found in the solution of Falle and Wilson (1985). Assuming the M87 jet is in the plane of the sky (more recent observations suggest an inclination of the jet-axis by only 17° (Walker et al., 2018; Akiyama et al., 2019)), for the chosen parameters, the placement of the shocks matches quite well with the spacing of the observed bright knots.

The jet reconfinement can also be driven by the pressure of its own cocoon. Here the problem is more complicated as the cocoon is a dynamic structure and its pressure evolves in time and so does the distance of the recollimation shock from the source and the jet radius after the reconfinement. In this regard the problem is qualitatively different from the less realistic one considered by Norman et al. (1982), where the jet is perfectly collimated already at the nozzle. The first simulations of initially conical non-relativistic axisymmetric hydro jets drilling their way through a uniform external gas was carried out by Falle (1991a). They used a shock-capturing second order Godunov scheme and their computational grid had 200×600 cells. These simulations have demonstrated that once the cocoon has expanded and its pressure dropped sufficiently to allow a significant increase of the jet radius after the recollimation compared to its radius at the nozzle, the overall evolution of the whole structure enters a phase of approximate self-similar behavior, where all its key parameters vary as power-laws

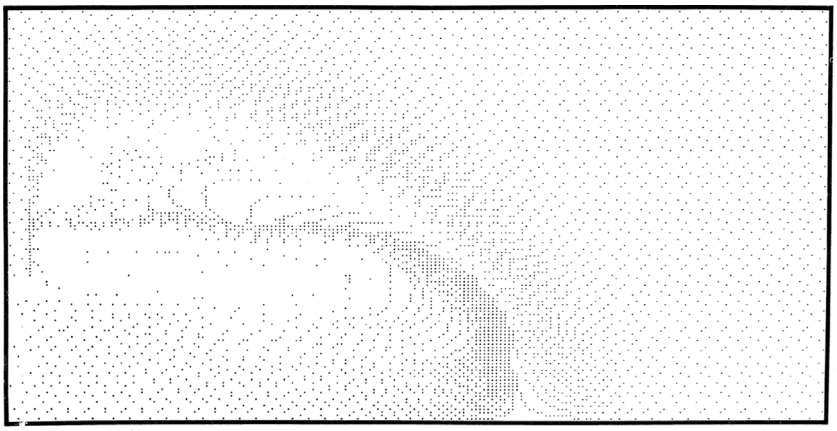

Fig. 1. Density visualization of the jet simulations by Rayburn (1977). One can make out the rarefied cocoon composed of jet material (marked with *-symbols), the forward bow-shock in the ambient medium (marked with +-symbols) and the termination shock of the beam.

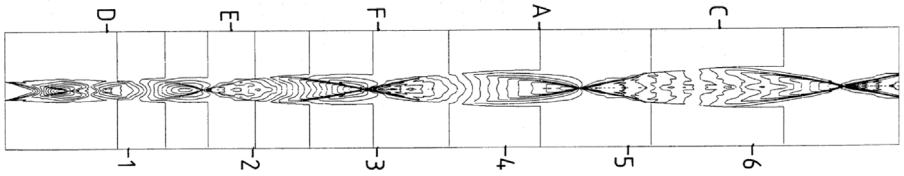

Fig. 2. Chain of reconfinement shocks compared to the observed spacing in M87 (capital letters) from Falle and Wilson (1985). Shown are pressure contours for an axisymmetric steady jet with $M_j(0) = 3.5$, $p_j(0) = 1.5p_0$ and $R_j(0) = 0.08r_c$, calculated on a 144 × 2192 grid. The observed position of the knows are marked on top, and the distance scale on the bottom is in units of the core radius r_c.

in time. The results were in accord with the analytic model presented in the same paper.

The fact that the AGN jets are magnetized and relativistic prompted the development of computer codes that could handle such flows. The first simulations of magnetized non-relativistic jets were carried out by Clarke et al. (1986). They used a numerical scheme for axisymmetric MHD which was a straightforward generalization of their earlier code for HD and evolved the poloidal magnetic field via the magnetic potential. The setup of their jet simulations was identical to that of Norman et al. (1982), but the injected flow carried out an azimuthal (toroidal) magnetic field which increased linearly with the distance from the axis. At the jet edge the ratio of magnetic and thermal pressures was $\beta = 0.2$. The computational grid had 600 × 100 cell and the simulations were carried out on a Cray X-MP supercomputer. The simulated jet did not produce the typical cocoon of its hydro counterparts as the shocked jet plasma was flowing not backwards towards the nozzle but forward where it formed a magnetically-pinched extended structure in front of the termination shock (dubbed the "nose cone"). Later, with the advent of the 3D era in computer simulations, it was shown that the nose cone was an artifact caused by the imposed condition of axisymmetry, which prevented the jet from developing of non-axisymmetric instabilities (Mignone et al., 2010).

The magnetic launching of jets in the context of disk accretion onto non-relativistic compact objects was first simulated by Uchida and Shibata (1985). Their initial setup involved a relatively thin radially unbalanced sub-Keplerian disk, surrounded by a uniform "corona". The whole configuration was threaded by a uniform magnetic field aligned with the rotational symmetry axis. As the simulations start, the inner unbalanced part of the accretion disk collapses, advecting the magnetic field towards the center and twisting it up in the process. The build-up magnetic pressure due to the generated azimuthal magnetic field then drives the less dense gas of the inner disk away in the form of a hollow collimated outflow. The authors commented that the process developed even for a Keplerian disk but at a slower rate. In this case, the accretion was driven by the vertical transport of the angular momentum facilitated by the large-scale magnetic field.

Relativistic fluids are more complex with tight interconnections between conserved variables and fluxes imposed by the covariant equations of their dynamics. For example, all types of energy, the rest mass-energy of particles, the thermal energy, the kinetic energy of bulk motion and the magnetic energy contribute to the inertial mass of fluid elements. A change in one component of the velocity vector modifies the momentum vector in all directions. This severely restricts the freedom of dealing with the transport of conserved quantities separately from one another, which exists in computational Newtonian fluid dynamics, and hence presents a new challenge (Norman and Winkler, 1986). An additional problem arises for numerical schemes whose design is based on the assumption of smoothness of solution. This is important because even initially smooth (or strong) solutions of compressible fluid dynamics can eventually develop discontinuities (weak solutions or shocks) via the nonlinear steepening of compression waves. In Newtonian fluids, this steepening can be limited via the method of artificial viscosity which introduces a strong additional flux term in the momentum equation. However, in relativistic fluids, the viscosity enters all components of the stress–energy–momentum tensor, including the energy and momentum density (Landau and Lifshitz, 1959). Hence any artificial modification of the momentum equation alone introduces inconsistencies which may result in arriving at nonphysical states (The same applies to other artificial ways of smoothing solutions, e.g. van Putten, 1993). After several attempts by various groups of researchers it was found that the most satisfactory performance was delivered by the so-called shock-capturing upwind numerical methods. These methods evolve all equations simultaneously, do not rely on artificial viscosity, do not require special treatment for weak solutions and extensively utilize the information on the causal connectivity between fluid elements. The first such schemes for relativistic HD were developed by Eulderink and Mellema (1994), Font et al. (1994) and Falle and Komissarov (1996) and for relativistic MHD by Komissarov (1999a). Readers interested in a more comprehensive review will find the paper by Font (2008) useful.

Understandably, many early simulations of relativistic jets were carried out more as trials of numerical schemes rather than as jet studies

and described just a single model (van Putten, 1993; Marti et al., 1994; Koide et al., 1996; Nishikawa et al., 1997). Others were focused on understanding the difference in dynamics of relativistic jets compared to their Newtonian counterparts and involved a parameterized set of numerical models (Yokosawa et al., 1982; Duncan and Hughes, 1994; Martí et al., 1997). The setup of these early simulations was identical to that of Norman et al. (1982). The issue of parametrization of the relativistic models is important for making a meaningful comparison with the Newtonian ones. For example, one may choose to use exactly the same parameters as in Norman et al. (1982), $\eta = \rho_j/\rho_e$ and $M_j = v_j/a_{s,j}$. In this case, given that $v_j \approx c$ and a_j is determined by the values of η and $p_j = p_e$, a small variation of M_j corresponds to large variation of the Lorentz factor. This results in a large variation of the jet ram pressure, $w\gamma^2 v$ (see Eq. (6)), and hence the advance speed of its head, leading to claims that relativistic jets are much more efficient "drillers" of the external medium. However, as the jet Lorentz factor is not an independent parameter here, the result simply indicates that this particular parametrization is rather unfortunate because it leads to the degeneracy of numerical models.

In fact, the parameter v/a does not have the same physical meaning in relativistic hydrodynamics as in the Newtonian one. In the Newtonian framework,

$$M = 1/\sin\theta_m\,, \tag{16}$$

where θ_m is the half-opening angle of the Mach cone. This cone defines the zone of influence of a point-like disturbance established by means of sound waves and hence the causal connectivity of supersonic flows. Using Eq. (16) to define the Mach angle in the relativistic framework, one obtains

$$M = \frac{v\gamma}{a\gamma_a}\,, \tag{17}$$

where $\gamma_a = (1-(a/c)^2)^{-1/2}$ (Konigl, 1980; Komissarov and Falle, 1998). Notice that like in the Newtonian case $M = 1$ implies $v = a$ but now M grows like γ in the ultra-relativistic regime. Sometimes it is claimed that relativistic jets have enhanced stability properties compared to Newtonian jets. This claim also arises from interpreting $v_j/a_{s,j}$ as the Mach number of relativistic jets. However, the actual Mach number given by (17) is normally much higher. When the correct definition is used, the claim of enhanced stability for relativistic flows becomes baseless (see Section 3.5).

A similar care has to be taken when defining the density-ratio parameter η. Which mass density should be used? This could be the proper rest mass density ρ (the mean rest mass of particles times their number density as measured in the rest frame of the fluid), the rest mass density as measured in the laboratory frame (the frame of the simulation) $\rho_1 = \gamma\rho$, the inertial mass density due to the rest mass of particles $\rho_2 = \gamma^2\rho$ or the total inertial mass density

$$\rho_3 = \gamma^2(w/c^2)\,, \tag{18}$$

where $w = \rho c^2 + e + p$ is the relativistic enthalpy. In principle, each of these quantities can be used for the purpose of parametrization of relativistic models. If however we wish to compare them with the Newtonian models, we need to remember that in the Newtonian physics the mass density is the inertial mass density and hence the relativistic models have to be parametrized using ρ_3, leading to the mass-density ratio parameter

$$\eta = \frac{w_j\gamma_j^2}{w_e}\,. \tag{19}$$

For a cold (in the relativistic sense) jet and external medium, one can ignore the thermal mass-energy and replace w with ρ. With the relativistic definitions (17), (19), the degeneracy of relativistic models is removed and the difference in the propagation efficiency and stability of relativistic and Newtonian jets is no longer that dramatic (Komissarov and Falle, 1996; Komissarov and Falle, 1998; Rosen et al., 1999).

While the jet trust $\Pi_j = \rho v_j$ determines the speed at which the head of a hypersonic jet advances through the external gas, the speed of the sideways expansion of its cocoon is determined by the rate at which it is supplied with the thermal energy by the jet, that is by the jet power L_j. From (2), (3), it follows that these are related as

$$L_j = \frac{v_j}{2}\Pi_j\,. \tag{20}$$

Thus given the same thrust, a faster jet inflates a bigger cocoon. This trend is already seen in the pioneering simulations by Yokosawa et al. (1982). In the relativistic hydrodynamics

$$L_j = c\,\Pi_j \tag{21}$$

(see Eqs. (5), (6)), showing that (20) extends quite well even into the ultra-relativistic regime.

The first numerical simulations of relativistic magnetized jets were carried out by Koide et al. (1996). They studied the propagation of a slab jet injected along a uniform external magnetic field of a uniform external medium. Later, the same problem was addressed using 3D simulations in the case of a cylindrical jet (Nishikawa et al., 1997). This problem is not particularly relevant to astrophysical jets but is more like a test problem for a numerical code. The magnetic field of astrophysical jets is much stronger than that of the external gas and it is expected to have a significant if not dominating azimuthal component. More realistic simulations were carried out by Komissarov (1999b), who studied the dynamics of axisymmetric jets with purely azimuthal magnetic field. Using the same settings as in the earlier Newtonian studies (Clarke et al., 1986; Lind et al., 1989), they focused on the conditions for developing the nose cone and also encountered the problem of appropriate jet parametrization in the process. Via analysis of relativistic MHD shocks, it was shown that the main jet parameter deciding the development of the nose cone was not the Newtonian magnetization parameter β but the relativistic parameter $\sigma = B_0^2/\rho_0$ (for hot flows $\sigma = B_0^2/w$), where B_0 is the magnetic field strength as measured in the jet frame. This conclusion was supported by the computer simulations carried out on a single processor workstation, with 300×1000 numerical grid, which demonstrated the development of substantial nose cones for $\sigma \gtrsim 0.1$.

The first attempt at the simulation of magnetic jet production in the context of general relativistic framework was made out by Koide et al. (1998, 1999). They considered a slender Keplerian disk around a non-rotating black hole surrounded by a rarefied corona. The whole domain was occupied by a magnetic field which was uniform at infinity (Wald, 1974) and aligned with the rotational axis of the disk. They used the 3+1 equations of RMHD adopted to the Schwarzschild coordinates of the hole's spacetime, which introduces a strong coordinate singularity at the event horizon, thus making the problem of finding accurate solutions near the horizon quite challenging. They described their numerical scheme as a Lax–Wendroff type scheme with artificial diffusion and did not say if any measures have been taken to preserve the magnetic field divergence-free. The axisymmetric computational grid had 217×71 points with the radial extension of the computational domain $[1.1r_s, 20r_s]$, where $r_s = 2GM/c^2$ is the Schwarzschild radius. The simulations were carried out on SX-4 supercomputers. The imposed magnetic field was strong enough to cause rapid loss of the angular momentum by the inner parts of the disk, the collapse of its centrifugal support and subsequent supersonic accretion. Somehow this catastrophic accretion was halted at about $r = 1.5r_s$ with a quasi-stationary shock forming around $r = 2r_s$. A similar phenomena was observed in their test simulations of an non-magnetized sub-Keplerian disk whose initial angular velocity was twenty percent below the Keplerian one. They attributed this halting of accretion to the centrifugal barrier effect. However, it is easy to verify that for such a disk the angular momentum is far too low and its inner part with r up to $\approx 8r_s$ should collapse into the black hole without encountering the barrier. Komissarov (2001b) reported that this was exactly what they observed during their attempt

to reproduce this result while testing their own GRMHD code. In spite of this controversy, the results of Koide et al. were encouraging as they included the development of a magnetically driven jet similar to the one observed in the earlier Newtonian simulations by Uchida and Shibata (1985).

The first known to us attempt to simulate the magnetic jet production in the context of magnetically driven accretion onto a rotating black hole was reported in 1999 by one of us at a conference on numerical methods. A brief description of this work was published only in the proceedings of this conference (Komissarov, 2001b) and has not been noticed by the astrophysical community. Yet, these simulations revealed a number of key features which were rediscovered later in more advanced studies and deserve mentioning here. The initial configuration described a marginally bound polytropic ($\hat{\gamma} = 4/3$) fat disk (Abramowicz et al., 1978) surrounded by a tenuous corona at rest relative to local zero-angular-momentum observers. The whole domain was threaded by a purely poloidal magnetic field. The disk interior was dominated by the gas pressure, with $\beta_{max} = 100$, whereas its outer layers and corona were magnetically dominated. The simulations were axisymmetric and used Boyer–Lindquist coordinates. The numerical grid was non-uniform with computational cells of approximately equal sizes in the r and θ directions. The domain extended in the radial direction from $r = 1.1r_+$ to approximately $150GM/c^2$. The numeric code was a generalization of the special relativistic code described in Komissarov (1999a). The simulations were rather short and terminated at $t = 800GM/c^3$. Only two models were presented, one for a non-rotating black hole and one for a rapidly rotating black hole with $a = 0.9$. In both cases, the magnetic torque was sufficient to initiate disk accretion and a relatively fast outflow with $v \approx 0.4c$ from the outer layers of the inner disk. In the non-rotating case, the highly magnetized funnel region near the symmetry axis developed fast accretion, with speed reaching $v = 0.9c$ near the inner boundary. In the rotating case, the inner part of the funnel region was still exhibiting an inflow but the outer part developed an outflow, with velocity reaching $0.8c$. This double-wind flow of the funnel was linked to the Blandford–Znajek mechanism of extracting the rotational energy of black holes (Blandford and Znajek, 1977). The simulations also allowed to identify a number of computational problems, which prevented the author from writing a proper paper to an astrophysical journal. Firstly, the flow through the inner boundary was not sufficiently fast to fully justify the use of the inflow boundary conditions at the inner boundary. Attempts to place the inner boundary closer to the horizon were unsuccessful due to the increased computational errors driven by the proximity to the coordinate singularity at the horizon. Secondly, over time the funnel flow developed very low density leading to eventual crashing of the simulations. All these issues raised doubts whether the claim of detection of the BZ process had a sufficiently firm basis.

3. Childhood

3.1. Blandford–Znajek mechanism and launching of relativistic jets from black holes

After the seminal theoretical work by Blandford and Znajek (1977), their electromagnetic mechanism of extracting the rotational energy of black holes was considered as one of the most interesting possibilities for powering the relativistic jets from AGN. The original theory was based on two asymptotic steady-state solutions of the force-free degenerate electrodynamics (FFDE) obtained in the limit of slow rotation. In this theoretical framework the inertia of plasma particles is completely ignored but their electric charges are accounted for in the same way as in a perfectly conducting medium. Due to the vanishing inertia, the electric and magnetic components of the Lorentz force completely balance each other, which explains why the system is called force-free. In the BZ solutions, this exotic model yields constant flux of the electromagnetic energy all the way from the event horizon to infinity, which is rather perplexing as the event horizon is causally disconnected from the outside world and any signal produced at the horizon cannot escape it. Hence in contrast to the surface of a neutron star, the horizon cannot play the role of a unipolar inductor. This property was at the core of the critic of the BZ mechanism by Punsly and Coroniti (1990). They argued that the steady-state solutions of Blandford and Znajek are lacking causal connectivity and cannot be sustainable in the time-dependent framework — in mathematical terms they must be globally unstable.

Punsly and Coroniti (1990) also proposed an attractive alternative where the inertia of plasma particles was paramount. In brief, the plasma is forced to rotate within the black hole ergosphere in the same sense as the black hole due to extreme case of the inertial frame dragging effect in this region. Because of the magnetic flux freezing of ideal MHD, the magnetic field is also dragged into the rotation. Hence in this picture it is the ergospheric plasma that plays the role of the unipolar inductor. This explanation seems rather odd as the plasma can be very rarefied, which suggests very low inertia. To this question Punsly and Coroniti had a very elegant answer. The magnetic field, they said, resists being dragged into the rotation around the black hole and pushes the plasma particles into the orbits with the slowest rotation possible. In the frame of local fiducial observers, who can be described as non-rotating with respect to the rotating space of the Boyer–Lindquist 3+1 spacetime splitting, such plasma rotates in the opposite sense to the black hole with almost the speed of light and hence has very high inertia. Moreover, it has negative redshifted energy (or "energy at infinity") and when it is swallowed by the black hole the hole's total mass-energy is reduced. Thus, the stationary total outflow of the redshifted energy starts near the horizon in the form of matter-dominated inflow of plasma with negative redshifted energy and ends in the form of magnetically-dominated outflow with positive redshifted energy outside of the ergosphere. The obvious analogy of this picture with the mechanical Penrose mechanism of extracting the rotational energy of black holes is the reason why it is often referred to as the "MHD-Penrose mechanism". One obvious drawback of this otherwise elegant theory was the lack of supporting analytic solutions. This meant that numerical experimentation was the only way of resolving this controversy.

In order to study the stability of the Blandford–Znajek solutions one has to work with the time-dependent formulation of FFDE. It turns out that its equations can be considered as a zero-inertia limit of relativistic MHD (Komissarov, 2002), which means that relatively straightforward modifications of a GRMHD code can turn it into a FFDE code. In order to have a clean numerical black hole experiment with low computational errors all the way down to the event horizon, one has to remove its coordinate singularity and hence not use the popular Boyer–Lindquist 3+1 splitting of the black hole spacetime. Fortunately, there are other ways to split the spacetime which do not introduce such a singularity and are yet asymptotically identical to the BL splitting at large distances. The first FFDE black hole experiments by Komissarov (2001a) were focused on the case of monopole magnetosphere, the simplest of the two cases considered by Blandford and Znajek (1977). The initial solution described a non-rotating radial magnetic field originating from the black hole. This field was winded in the azimuthal direction in order to ensure that the perfect conductivity condition is satisfied inside the ergosphere. The Kerr–Schild spacetime splitting allowed to put the inner boundary of the computational domain inside the outer horizon, in the region which is causally disconnected from the outside space, and use the radiative boundary conditions on it. As soon as the simulations began, the magnetosphere started to rotate and a strong spherical switch-on wave moved from the black hole into the surrounding space. This was not a simple unwinding of the initial twist as behind the wave the magnetic field remained twisted and rotating. Moreover, in this region the solution quickly settled to a steady-state with an outgoing Poynting flux. In the case of slowly rotating black holes, the steady-state was in excellent agreement with the asymptotic

solution of Blandford and Znajek. This proved that this solution was asymptotically stable and hence physically meaningful. The underlying physics of the mechanism was later clarified in Komissarov (2004a, 2009).

Even if the FFDE solution was meaningful, it was still important to demonstrate that inclusion of particle inertia does not result in a qualitatively different behavior. Moreover, in context of the accretion disk simulations, the double-wind nature of the BZ-type solution in the disk funnel naturally leads to it being drained of matter. This caused MHD codes to crash unless the matter is artificially resupplied in situ. Although this imitates the physical processes of particle creation as discussed in Blandford and Znajek (1977), one has to demonstrate that the artificial injection does not corrupt the numerical jet solutions. In order to address these issues, Komissarov (2004b), repeated the simulation of the monopole magnetosphere but now within the GRMHD framework. The results demonstrated that for the degree of magnetization which can be achieved in GRMHD schemes with reasonably high resolution, (1) the electromagnetic part of the MHD solution stays quite close to the BZ solution; (2) within the ergosphere the plasma is not pushed into orbits with high Lorentz factor and hence its inertia remains small, in contrast to what is envisioned in the MHD-Penrose process; (3) the in situ injection of matter can be done in the way that does not corrupt the electromagnetic solution.

These results were at odds with the MHD simulations by Koide et al. (2002), Koide (2003) who considered a different magnetic configuration which describes an asymptotically uniform magnetic field aligned with the rotational axis of the black hole, just like in Koide et al. (1998, 1999) but without the accretion disk and using the same numerical scheme. They claimed that the ergospheric plasma acquired negative redshifted energy and that the rotational energy of the black holes was extracted via the MHD-Penrose process. However, they run their simulations only for very short time $t \approx 13GM/c^3$. Later, these simulations were repeated using an upwind conservative code which utilized the horizon-singularity-free Kerr–Schild coordinates (Komissarov, 2005). The resolution was twice as high and the simulations run until $t = 60GM/c^3$. Their results also exhibited the development of a region inside the ergosphere where plasma had negative redshifted energy but only during the transient initial phase. During this phase some of the magnetic field lines crossing the ergosphere did not cross the outer horizon but had a turning point in the equatorial plane and the negative redshifted energy was seen only around these turning points. Eventually, all such field lines were "accreted" by the black hole. The current sheet that developed in the equatorial plane of the ergosphere was subject to magnetic reconnection indicating that some interesting physics may take place there when the perfect conductivity condition brakes down (see Komissarov, 2004a; Parfrey et al., 2019). However, in accreting black holes this part of the ergosphere will be dominated by the dense disk plasma plunging into the black hole.

Outflows driven by the BZ mechanism were also not identified in otherwise very impressive GRMHD simulations of accretion disks by De Villiers et al. (2003, 2005) where angular momentum transport is promoted by the turbulence arising from the magneto-rotational instability (MRI). Their initial configuration involved a torus with a poloidal magnetic field aligned with the torus isodensity contours and an unmagnetized tenuous gas around it. As the simulations progressed, a highly magnetized funnel developed in the polar region above the black hole where one would expect the BZ mechanism to drive a relativistic outflow, like found earlier in Komissarov (2001b). However, inside the funnel they saw only a thermally accelerated outflow heated "by shocks driven into the funnel by the accretion disk and corona" (De Villiers et al., 2003) and concluded that a process similar to the MHD Penrose mechanism was powering the denser outflow at the funnel wall (De Villiers et al., 2005). Their computer code was neither conservative nor fully upwind and relied on the artificial viscosity method to deal with weak solutions. They also used the Boyer–Lindquist splitting of the spacetime, with its horizon singularity. These could be the reasons behind the failure to capture the BZ-powered outflow.

Later, simulations with a very similar setup to those of De Villiers et al. (2003) were carried out by McKinney and Gammie (2004a), using an upwind shock-capturing code HARM which utilized the Kerr–Schild splitting of the black hole spacetime. In this computational experiment, it was possible to firmly identify the BZ mechanism as the process powering the highly-magnetized funnel outflow. This paper marks a turning point from a period of uncertainty and controversy to a period of wide acceptance that the Blandford–Znajek mechanism can be captured in GRMHD simulations of the black holes and that it does naturally drive highly-magnetized collimated outflows in the context of disk accretion onto rotating black holes. From this point onward, the computational studies of the BZ process have been focused mainly on the question of how much magnetic flux can be accumulated in the black magnetosphere and hence how powerful the black hole jets can be. Recalling the energy extraction due to Blandford and Znajek, $P_{\rm BZ} \propto \Phi_{\rm BH}^2 a^2$ which is valid in the low spin regime (see Tchekhovskoy et al., 2010a for more general expressions), the jet power depends critically on the amount of magnetic flux threading the horizon $\Phi_{\rm BH}$. The latest results suggest that the maximum magnetic flux is reached when its magnetic pressure is approximately balanced by ram-pressure of the accretion flow (Tchekhovskoy et al., 2011; McKinney et al., 2012). Appropriately normalizing the flux by the accretion rate $\phi_{\rm BH}^2 = \Phi_{\rm BH}^2/\dot{M} r_{\rm g}^2 c$ numerical studies have found a saturation value of $\phi_{\rm BH} \sim 30 - -60$ which depends mostly on black hole spin and somewhat on the scale-height of the disk, where taller disks can sustain larger fluxes on the black hole horizon (Tchekhovskoy et al., 2012). In this so-called "magnetically-arrested-disk" regime (MAD), the BZ power of black-hole jets is hence directly proportional to the accretion power $\dot{M}c^2$ but can exceed the latter considerably, with 300% being the current maximum achieved (McKinney et al., 2012). This super-efficiency of MADs is the strongest evidence that energy can indeed be extracted from a rotating black hole as envisioned by Blandford & Znajek.

3.2. Black Hole-torus simulations

The GRMHD simulations of Black Hole jets mentioned above have been so influential in our understanding of the jet phenomenon that they deserve a more detailed discussion. Given that jets in nature are typically observed in states of radiatively inefficient accretion, the impact of radiation is typically neglected in Black Hole-torus simulations. In this scenario, a hydrodynamic equilibrium torus with temperatures close to the virial one (Fishbone and Moncrief, 1976; Kozlowski et al., 1978) is initially perturbed with a weak magnetic field of varying topology. The magneto-rotational instability (MRI), first applied in the context of accretion disks by Balbus and Hawley (1991) then kicks in and provides turbulent Maxwell and Reynolds stresses, driving angular momentum transport and accretion. The fact that viscosity arises naturally out of the MHD turbulence is one of the great virtues of the model. After the initial excitement, the first problems with the model started to occur: despite the turbulence in the disk, whether at all or how powerful a jet would be launched from the black hole depended critically on the initial conditions. Large initial vertical flux was shown to yield the strongest jets (McKinney and Gammie, 2004b; De Villiers, 2006) and fields with smaller coherence length would produce jets weaker by a factor of a few or only transient outflows. This memory of the initial field configuration is largely determined by the ideal MHD assumption which disallows a topological rearrangement of field-lines (for example, a single magnetic field loop cannot split into two). In computer simulations of the ideal MHD system, such rearrangement or "reconnection" of field lines only occurs through numerical error.

These initial studies were in axisymmetry, but the situation would not substantially improve for full 3D simulations (Beckwith et al., 2008). Toroidal field initial configurations producing jets were reported by McKinney et al. (2012) but the jets were only short lived with a duty

cycle of $\sim 2\%$ and average power of 0.01% compared to the accretion power. These transient jets rapidly dissipated after a distance of $\sim 50\ GM/c^2$ and could not serve as models for powerful jets. However, it is quite natural to assume a toroidal field configuration for accretion flows in various contexts: orbital shear in an X-ray binary or a tidal disruption event would predominantly amplify the toroidal magnetic field and a purely toroidal configuration seems a natural starting point for the simulations. Hence the problem of magnetic flux generation and transport has become one of the key issues in understanding black hole engines (Sikora and Begelman, 2013).

The reason for the absence of a persistent jet in McKinney et al. (2012) and similar studies Beckwith et al. (2008) was sought in the weak amplification of the poloidal field due to the MRI which in addition becomes exceedingly hard to resolve with decreasing field strength. It took simulators ten years to achieve the necessary resolutions and finally report self-generation of the poloidal magnetic field due to an α-effect by Liska et al. (2020). Though the initial magnetization of the disk was rather high (the initial uniform magnetic pressure was set to 20% of the thermal pressure) the proof of principle is an important milestone as it shows that strong jets, in their case surpassing the accretion power by $\sim$ 140%, can emanate even from purely toroidal initial field configurations.

With the widespread application of conservative numerical schemes for general relativistic magnetohydrodynamics, a large consensus in the simulation of "standard" Black Hole-torus simulations has emerged. In particular, the level of agreement in a scenario leading to moderate magnetic flux on the horizon (coined Standard And Normal Evolution "SANE" by Narayan et al. (2012)) has recently been assessed in a code comparison effort led by one of the authors (Porth et al., 2019) whereby nine independent groups performed simulations of identical initial conditions at varying resolutions. Despite the chaotic nature of the turbulent problem, key qualitative aspects of the accretion process and formation of a BZ jet are recovered by all teams. On the quantitative side, as soon as sufficient resolution to continuously resolve the MRI is given, all codes agree on diagnostics like accretion rate and dimensionless flux $\phi_{\rm BH}$ within the turbulent fluctuations. It should be noted that in this comparison effort, convergence was probed up to an unprecedented level with an equivalent of 1024^3 zones, surpassing previous studies by a factor of $\times 2.75$ in linear resolution (corresponding to 20 times more computational zones!).[1] The benchmark of Porth et al. (2019) shows the strengths and weaknesses of state-of-the-art numerical simulations of black hole accretion and jet formation: while the simulations are mature enough to constrain certain parameters of the observations as performed by the Akiyama et al. (2019), large uncertainties of $\sim$ 20% still exist in predictions of the jet opening angle from simulations. In addition, full convergence of the turbulent α stress parameter has not yet been demonstrated as the Maxwell stress increases with numerical resolution (as opposed to local shearing box simulations where it is found to decrease with resolution Bodo et al., 2014; Ryan et al., 2017; Guan et al., 2009).

A second flavor of the radiatively inefficient accretion black hole-torus system is recovered for initial conditions with large amount of magnetic flux. If flux can be effectively transported from larger radii, the magnetic field strength increases due to the decreasing surface area and its accumulating pressure will ultimately halt the accretion process, forming a MAD (Bisnovatyi-Kogan and Ruzmaikin, 1976; Narayan et al., 2003). First simulations of this highly magnetized state were presented by Igumenshchev (2008) using a pseudo-Newtonian approach, and GRMHD simulations followed shortly thereafter (Tchekhovskoy et al., 2011; McKinney et al., 2012). An important finding of these simulations is that, once a MAD regime is reached, the saturation flux $\Phi_{\rm BH}^2 \propto \dot{M} r_{\rm g}^2 c$ is independent of the *initial* flux distribution in the disk. How much flux a given accretion disk can hold on the black hole depends only on its scale height which leads to a direct relation between BZ jet power, accretion rate, black hole spin and scale height (Tchekhovskoy et al., 2012).

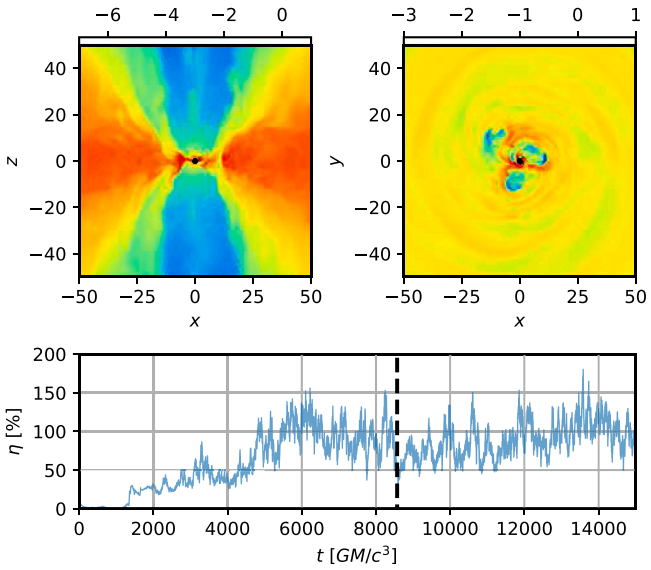

Fig. 3. Visualization of a GRMHD simulation showing magnetically arrested disk accretion (MAD). The top panels show logarithmic rest-frame density on slices across the $xz-$ and xy-planes. Three flux-tubes of low density have detached from the black hole horizon and orbit along with the disk plasma (top right). In the bottom panel we show the jet efficiency which temporarily reaches 150% of the accretion luminosity. The vertical dashed line indicates the time of the snapshot. The simulation was performed with BHAC (Porth et al., 2017).

Due to the strong fields present in the inner regions of MADs, the MRI is suppressed as the fastest growing wavelength $\propto v_a/\Omega$ becomes larger than the disk scale-height. Furthermore, the strong magnetic pressure of the central field opposes accretion of matter altogether. Axisymmetric simulations (Igumenshchev, 2008) hence show a bursty behavior with mass first accumulating at the magnetospheric radius and then cyclically breaking through to the black hole. The dynamics in 3D is entirely different: magnetic flux bundles are found to erupt from the black hole due to interchange with denser disk plasma and magnetic reconnection. Accretion then proceeds in spiral streams through islands of strong magnetic flux. This is illustrated in Fig. 3 which also shows the jet efficiency reaching 100% and above. As the MRI is suppressed, what drives accretion in the MAD regime is not fully understood. The possibilities are turbulent stresses due to Rayleigh–Taylor interchange instabilities or large-scale Blandford & Payne-type torques (Blandford and Payne, 1982) of the orbiting flux bundles (Marshall et al., 2018). Overall, as MAD regimes present harder challenges to the numerical codes, such simulations have become only quite recently accessible to a wider community. To demonstrate to which extent the results agree between different numerical treatments is an important outstanding task.

3.3. Launching jets from accretion disks

In young stellar objects, jets form as a by-product of the accretion process, giving rise to the Herbig–Haro objects (see Chapter "Jets in Young Stellar Objects" of this volume). The key mechanism of jet formation from accretion disks was described by Blandford and Payne (1982) as a self-similar solution to the MHD equations. The first simulations showing formation of jets as magnetized outflows from accretion disks were presented twenty years later by Casse and Keppens (2002, 2004, Fig. 4). In their axisymmetric setup, a thin accretion disk is permeated by an hour-glass shape magnetic field configuration. Inclusion

[1] Data publicly available under http://datacommons.cyverse.org/browse/iplant/home/shared/eht/2019/GRMHDCodeComparisonProject.

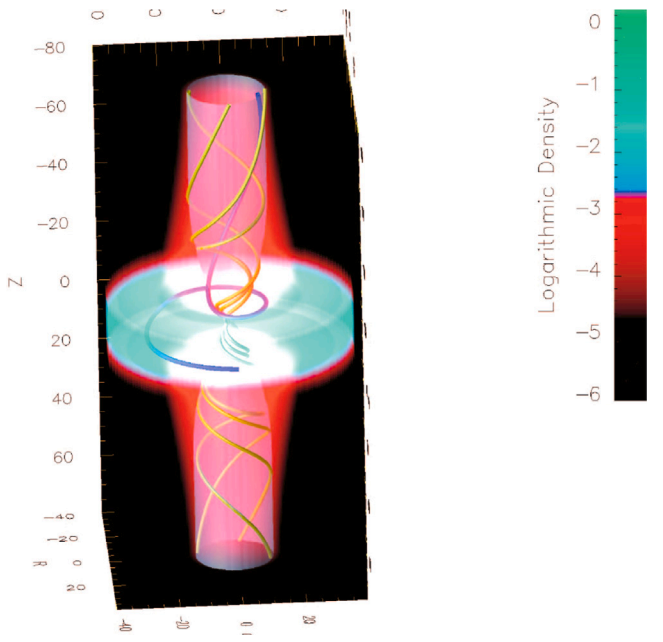

Fig. 4. Three-dimensional impression of the final near-stationary end state reached in the disk-jet solutions from Casse and Keppens (2004). Color levels represent a volume rendering of plasma density, and translucent surface stands for a magnetic surface anchored at $R = 3$ in the disk. Yellow and blue lines stand for magnetic field lines and flow streamline, respectively. Magnetic field lines are twisted by disk rotation, which provokes mass acceleration as shown by the flow streamline that is initially accreting towards the central object and then turns into the jet. (For interpretation of the references to color in this figure legend, the reader is referred to the web version of this article.)

of anomalous plasma resistivity characterizing unresolved turbulence in the simulation allows for matter to cross magnetic field lines and thus one fraction of disk-plasma accretes onto the central object and another fraction (roughly 20% in Casse and Keppens, 2004) is diverted to the outflow. In the ensuing near stationary state, the force-balance along and across the magnetic field lines can be investigated, confirming the role of hoop-stress in collimating the (Newtonian) jet. Numerical setups in the tradition of Casse and Keppens (2002) have been extensively studied for the role of the involved parameters: diffusivity and field strength (e.g. Zanni et al., 2007; Tzeferacos et al., 2009; Sheikhnezami et al., 2012), viscosity (Murphy et al., 2010) and heating (Tzeferacos et al., 2013).

These studies have shown that the steady jet launching due to magneto-centrifugal forces occurs for a much wider range of the disk magnetization than previously thought based on simplified analytic calculations. Self-similar solutions suggest that jets accelerating to super-Alfvénic speeds can only be launched in disks with mid-plane magnetization $\mu = B^2/2p$ close to equipartition (Li, 1995; Ferreira, 1997). Numerical simulations, relaxing key assumptions on the "cold" or "adiabatic" disk thermodynamics however have demonstrated stable jet launching in a range of $\mu \approx 0.001 - 0.3$ (Tzeferacos et al., 2009; Murphy et al., 2010; Sheikhnezami et al., 2012; Stepanovs and Fendt, 2014). Whether such disk jets can also be launched with magnetization substantially above unity and thus potentially reach relativistic speeds remains to be shown.

In a first study by Tzeferacos et al. (2009), higher disk-magnetizations indicated stronger mass-loading of the outflow and higher ejection-to-accretion ratios, disfavoring generation of fast outflows with high magnetization. Using simulations that undergo sequences of stationary states and investigating correlations of outflow quantities with the momentary disk magnetization, Stepanovs and Fendt (2016) however show the opposite trend: the asymptotic outflow velocity increases with magnetization and the mass-loading decreases. The change comes about as the simulations of Stepanovs and Fendt (2016) last for much longer and thus more faithfully capture a stationary state. Despite these advances, the generation of Poynting flux dominated outflows as required for relativistic AGN jets remains to be demonstrated.

In the relativistic regime, the collimation and acceleration of winds emitted from disks was first numerically studied by one of the authors in special relativity (Porth and Fendt, 2010). As the simulations started from a hot rotating corona above the disk (similar to previous Newtonian studies Ustyugova et al., 1995; Ouyed and Pudritz, 1997) and did not include the launching of the flow near the mid-plane, the mass-loading could not be investigated self-consistently. The main focus of the study is the collimation of flows in the trans-relativistic regime. It was shown that disk winds can collimate via hoop stress before reaching the fully relativistic regime beyond the light-cylinder where acceleration and collimation becomes inefficient (see Section 3.4).

With general relativistic resistive magnetohydrodynamic codes (e.g. Bugli et al., 2014; Qian et al., 2017; Ripperda et al., 2019), disk-jets can now be modeled in full general relativity and the relative contributions of the disk and black hole jet evaluated separately (Qian et al., 2018; Vourellis et al.). While it has been shown that the energy flux from the disk can dominate over the black hole driven jet, so far only mildly relativistic velocities $\sim 0.1c$ have been reported from the disk. Given the large and unconstrained parameter space of plasma (anisotropic) resistivity, disk thermodynamics, viscosity and magnetic field structure, disk jets might still be in for a surprise though!

3.4. Acceleration and collimation

The question of whether jets are able to magnetically self-collimate has been debated for many years, in particular in the relativistic case. In principle, the asymptotic collimation of the inner flow lines to the axis has been shown from theoretical considerations (Heyvaerts and Norman, 1989, 2003; Chiueh et al., 1991; Appl and Camenzind, 1993; Bogovalov, 1995), however it was found that the involved scales are exponentially large (Eichler, 1993; Tomimatsu, 1994; Lyubarsky, 2009). Hence whether collimation is possible on astrophysically relevant scales is not obvious.

That magnetic jet acceleration is tightly connected to the collimation of the flow lines can be understood from an analysis of the stationary MHD equations with very few assumptions. It turns out that for a cold flow beyond the light-cylinder, the Lorentz factor increases as the so-called bunching function $S = B_p R^2$ decreases (where B_p is the poloidal field strength and R the cylindrical radius) (Begelman and Li, 1994; Bogovalov, 2001; Vlahakis and Königl, 2003; Tchekhovskoy et al., 2009). Acceleration can hence be achieved via *differential* collimation that is obtained when the inner field-lines collimate faster than the outer ones. More precisely, the separation ΔR between two magnetic flux surfaces has to increase faster than the cylindrical radius R, resulting in a so-called *magnetic nozzle* (Begelman and Li, 1994). Hence to solve for the jet acceleration, knowledge of the jet shape is of fundamental importance.

The collimation of the jet is governed by the Grad–Schlüter–Schafranov (GSS) equation of the forces across the flux surfaces. The solution to this second-order non-linear elliptic partial differential equation is already complex in the Newtonian case. For relativistic flows, it is further complicated by the fact that the electric field, which is safely neglected in the Newtonian context, nearly cancels with the collimating force from the current (Bogovalov, 2001; Vlahakis and Königl, 2003). With the two dominating terms closely balanced, finding accurate analytical solutions to the stationary equations is very challenging. In fact, which terms in the trans-field equation remain asymptotically relevant has been in question until clarification from numerical simulations was provided. For example (Chiueh et al., 1991; Lyubarsky and Eichler, 2001; Okamoto, 2002), omitted the centrifugal term in their analytic calculations, while (Bogovalov, 1995; Beskin and Malyshkin, 2000; Tomimatsu and Takahashi, 2003) instead omitted the

poloidal curvature term. Naturally, the acceleration behavior depends critically on the dominant terms. When the poloidal curvature force is neglected, an efficient *linear acceleration* is recovered $\gamma \approx r/r_{\rm ls}$ (Contopoulos and Kazanas, 2002). However, with the poloidal curvature dominant, the acceleration is more delicate and results in the so-called *powerlaw* acceleration regime (see e.g. Romero and Vila, 2014, for a comprehensive review).

Numerical simulations by Komissarov et al. (2007, 2009) and Tchekhovskoy et al. (2009) played an important role to settle the question of magnetohydrodynamic jet acceleration and self-collimation. Unlike previous attempts who were seeking stationary solutions of the wind- and GSS-equations (e.g. Camenzind, 1987), these authors used the set of hyperbolic time-dependent relativistic MHD equations and let the solution settle into a stationary state. This set of equations is in principle much easier to handle, but to be successful two major numerical challenges had to be overcome: 1. to accurately follow conversion of energy into kinetic form, numerical schemes of low dissipation are required. This problem was countered with specially designed flow-aligned grids in elliptical coordinates. 2. As the scales involved in the jet acceleration are extremely large, a brute force approach covering more than six orders of magnitude stands little chance. Thus, using the fact that most of the jet acceleration proceeds in the super-fast magnetosonic regime, the grid can be split up into sectors of increasing size which are consecutively advanced to a stationary state with increasing local timesteps. This grid-extension technique allowed for the first time to find stationary solutions of jet-acceleration and collimation covering six to nine orders of magnitude in spatial scales. Careful analysis of the simulations showed that relativistic jets in AGN can be efficiently accelerated by magnetohydrodynamic processes reaching equipartition within the parsec-scale. In application to GRBs, MHD acceleration can provide ultra-relativistic Lorentz factors of $\gamma \sim 100$ at distances from the central engine of 10^{10}–10^{12} cm, well within the tentative distance of the prompt emission of $\sim 10^{13}$ cm as inferred from burst variability (e.g. Piran, 2004).

While a full discussion can be found in Komissarov et al. (2009), we here just summarize the findings of the numerical jet acceleration/collimation studies. Efficient acceleration in the linear regime requires external pressure to aid in jet collimation with $p \propto z^{-\alpha}$ and $\alpha < 2$. For $\alpha > 2$ the flow looses causal connectivity and ballistically expands with conical shape. The case $\alpha = 2$ is less clear, as the collimation depends on the condition of the flow before entering the asymptotic region, but the collimation becomes poor, $z \propto r^a$ with $1 < a \leq 2$ and acceleration is inefficient.

As discussed above, differential collimation yields MHD acceleration for confined flows due to differential field-line bunching. At the same time, de-collimation can also lead to a reduction of $r^2 B_p$ and thus provide a means to accelerate a jet. In fact, rapid de-collimation due to loss of confining pressure is expected when a collapsar jet leaves the remnant of the host-star. This effect was found in numerical simulations by Tchekhovskoy et al. (2010b) and confirmed by Komissarov et al. (2010) who coined the term *rarefaction acceleration* due to the conceptual similarity with a 1D Riemann problem previously considered by Aloy and Rezzolla (2006) and Mizuno et al. (2008). An illustration of the typical collimation/acceleration studies is shown in Fig. 5 where an ultrarelativistic jet is confined to a given boundary of varying shape. The rarefaction acceleration is shown on the right-hand panel yielding a substantial increase of the Lorentz-factor in particular at the boundaries of the jet where the solution changes most dramatically.

3.5. Jet instabilities

The steady-state analytic or semi-analytic models of jets normally have a very simple structure and are by definition "lifeless". They may be useful for understanding some of the basic processes behind the observed dynamics of real jets but often they bear little resemblance with the actual natural phenomena. The problem is that the symmetry assumptions, including the time-independence, throw away many other processes which ultimately determine what we actually see. For example, a steady state model of a pressure-matched cylindrical jet in a uniform external gas may describe a flow which remains completely unchanged along its direction of motion, whereas the real jet exhibits a transition to a fully turbulent state. Obviously, this issue is not restricted to astrophysical jets but to most phenomena of life and nature.

What usually renders theoretically constructed steady-state solutions almost void are instabilities or waves of growing amplitude. They may start as small perturbations but eventually grow strong, dramatically modifying the initial solution in the process. In the astrophysical context, another potentially very important role of the instabilities is that they may trigger strong dissipation of both the kinetic energy of bulk motion and the magnetic energy, thus paving the way to the production of the observed emission (see Perucho, 2019 for a recent in-depth review). The "engines" of astrophysical jets appear to be unsteady as well, contributing to the complexity of the flows they produce. This unsteadiness may also be a result of instabilities. Moreover, instabilities could be essential even in the very functioning of these engines.

The instability studies usually start from the linear stability analysis, which for a cylindrical jet deals with small perturbations of the form

$$f(r)\exp(i(m\phi + kz - \omega t))$$

where m is the azimuthal wavenumber, $k = 2\pi/\lambda$ is the axial wavenumber and ω is the angular frequency. In the so-called temporal approach, one may fix real values of m and k, but $f(r)$ and complex ω are to be found as solutions to an eigenvalue problem. In the spatial approach, one fixes real ω and looks for the complex eigenvalue of k instead. Normally, these eigenvalue problems are rather complicated and have to be solved numerically. Typically, more than one unstable solution exists, corresponding to modes of different types. On the ω–k dispersion diagram they appear as different branches. A nice concise discussion of the approach with clear illustrations can be found in Baty (2005).

Like their laboratory counterparts, astrophysical jets can suffer from the Kelvin–Helmholtz instability, which is fed by the kinetic energy of their bulk motion. In the case of jets one can distinguish ordinary or surface modes whose amplitude rapidly decays away from the surface and global body modes which occupy the whole of the jet body (Birkinshaw, 1991). The body modes appear only for supersonic jets and they are fed via the so-called resonant reflection of sound waves off the jet surface, where the reflected wave is stronger than the incident one (Miles, 1957; Payne and Cohn, 1985). Their growth mechanism involves repeated bouncing off the opposite sides of the jet, and hence relies on the causal communication across the jet.

Naturally, the results of the stability analysis depend on the exact structure of the steady-state solution. For a uniform jet, the most rapidly growing global resonant mode of the KHI has the wavelength

$$\lambda_{KH} \approx \frac{2\pi R_j M_j}{2/3 + \eta^{1/2}}\,, \tag{22}$$

where R_j and M_j are the jet radius and Mach number respectively and η is the ratio of inertial mass-energy densities of the jet and external gas in the laboratory frame (Hardee, 1987a,b). For a jet emerging from a nozzle it is better to consider the spatial growth of the instability. The corresponding e-folding length scale is

$$l_{KH} \approx R_j M_j\,. \tag{23}$$

The result applies both to Newtonian and relativistic jets, provided one uses the relativistic definitions of the Mach number (Eq. (17)) and inertial mass density (Eq. (18)) (Hardee, 1987b; Bodo et al., 2004).

The linear phase of an instability is difficult to detect observationally as in this phase the perturbations are very small. However, the subsequent nonlinear phase and saturation phases are no longer

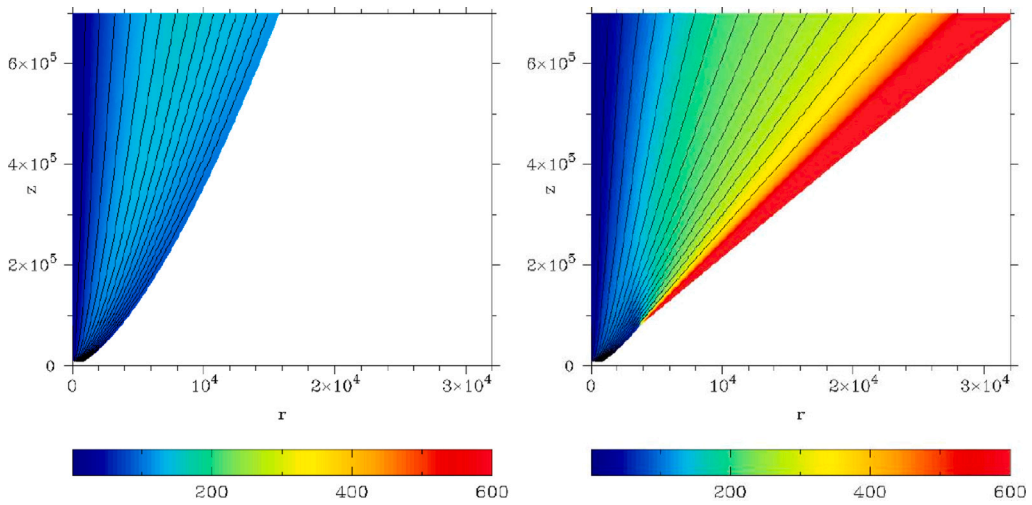

Fig. 5. Collimation/acceleration study of Komissarov et al. (2010) showing the jet Lorentz factor in color and the magnetic field lines as black contours. In the left panel, the jet is confined by a funnel with shape $z \propto r^{3/2}$. In the right panel, the funnel suddenly becomes conical at $z = 7 \times 10^4$ inlet radii (mimicking the escape of the jet from the stellar remnant in a long GRB). The unconfined jet solution rapidly expands leading to "rarefaction acceleration" as the separation between flux tubes increases faster than the cylindrical radius.

described by the linearized equations and in order to study the observable consequences of instabilities one has to resort to the method of computer simulations. They show that while the surface modes lead to the development of a turbulent boundary layer, the body modes may result in large-scale distortions of the jet and quickly lead to its total disruption (Bodo et al., 1994; Perucho et al., 2004, 2005). This is particularly true when the external gas is heavier than the jet as in this case displacing external gas takes more energy. In the relativistic case, the jets should be classified as light or heavy based on their inertial mass-energy density $\rho = \gamma^2 w$ (see the discussion in Section 2), or one risks arriving to confusing conclusions.

The astrophysical jets are magnetized and it looks increasingly likely that most of them are launched via a magnetic mechanism. As far as jet instabilities are concerned, the role of the magnetic field is two-fold. On the one hand, the magnetic tension resists deformations along the field-lines which may inhibit the development of non-magnetic instabilities. The higher the curvature radius of the deformation, the stronger is the restoring magnetic force. This explains why the magnetic inhibition is stronger for short-wavelength modes, which can be suppressed altogether (Appl and Camenzind, 1992; Ferrari, 1998). On the other hand, new instabilities, now fed by the magnetic energy, can grow. Associated with the $\mathbf{J} \times \mathbf{B}$ force, these are called current-driven instabilities (CDI).

Initial studies of CDI were driven by thermonuclear fusion programs. These were focused on static plasma columns separated by a vacuum region from the container walls. A cylindrical configuration of the type is found to be unstable to the modes satisfying the Kruskal–Shafranov criterion

$$\frac{kRB_z}{B_\phi} > 1\,, \tag{24}$$

where R is the radius of the column. The modes are essentially standing waves. In the jet context, the CDI modes do not propagate in the fluid frame but are simply advected by the flow (Appl et al., 2000). In the fluid frame, the maximum temporal growth rate is about

$$\tau_{CD} \approx \frac{2\pi P}{c_a}\,, \tag{25}$$

where c_a is the Alfvén speed and $P = RB_z/B_\phi$ is the distance along the jet required for one full turn of the magnetic helix, called the magnetic pitch (Appl et al., 2000). The corresponding e-folding linear scale is

$$l_{CD} = 2\pi P M_a\,, \tag{26}$$

where M_a is the Mach number with respect to the Alfvén speed. With the relativistic definition of the Mach number, Eq. (26) can be used for the relativistic jets as well as for the Newtonian, provided the pitch is treated as measured in the fluid frame. Strictly speaking, these results apply only in the case of constant pitch across the jet and top-hat velocity profile, whereas the steady-state equations describing the equilibrium of a cylindrical magnetized jet allows infinitely many solutions with very different radial profiles for all fluid parameters, which explains the large number of studies concerning the linear growth of CDI.

The fluid jets studied in laboratories or produced by rocket engines do not last for more than a hundred radii of the jet engine nozzle. In good agreement with the stability theory, they are destroyed by the Kelvin–Helmholtz instability. In contrast, the jets from AGN and young stars manage to survive for much longer. In the case of black hole jets, the initial jet radius is about few times the gravitational radius of the black hole, which is about $10^{14} M_9$ cm for a mass normalized to a typical value $M_9 = M/10^9 M_\odot$ of the supermassive black holes residing in the center of AGN. In some cases, the AGN jets can be traced up to a distance of 1 Mpc, which is about 10^{10} initial jet radii. If the jet of rocket engines had such survivability, they would be able to reach the Moon! The jets from young stars are equally impressive in this regard. What makes them so special? If we apply the growth rates for KHI and CDI given by Eqs. (23) and (26) replacing R_j with the jet radius at its source, the expected maximum jet length would be much shorter compared to the observations, unless the Mach numbers are "astronomically" high, reaching $M \approx 10^9$ in some cases.

The explanation to the apparently incredible stability of astrophysical jets seems to reside in the fact that they are not infinitely collimated cylindrical flows but flows with measurable finite opening angle and hence their radius increases significantly with the distance from the source. This sideways expansion can be the indication of a decreasing external pressure confining the jets or even its inability to confine the jets altogether. Hardee (1987b) modeled the spacial growth of KHI in expanding jets confined by external pressure $P \propto z^{-a}$ assuming that the local growth rate is the same as in the cylindrical jet with the same flow parameters. He found a significant reduction of the overall growth. Moreover, for $a = 2$ the perturbation amplitude it is no longer an exponential function of the distance but a power law and for $a > 2$ its growth quickly comes to halt. In fact, for $a > 2$ initially pressure-matched jets eventually become free-expanding as sound waves can no longer provide causal communication across the jet (Lyubarskij, 1992; Porth and Komissarov, 2015). Thus, the predictions of Hardee's model seem reasonable, but the model still had to be verified somehow and numerical simulations are the most suitable approach for this.

Rosen and Hardee (2000) used 3D simulations to study the stability of magnetized conical non-relativistic jets. Their results were in line with the expectations, but the expansion rate was rather low to have a strong effect. The results did not indicate that jet instability can be suppressed altogether.

A number of other simulations addressed the problem of stability of expanding jets. Since the very important kink modes are non-axisymmetric, it is essential for such simulations to be three-dimensional and hence computationally intense. The setup of the 3D Newtonian simulations of Moll et al. (2008) allowed to address the issue of stability not only in the context of jet propagation but also in the context of jet launching. Their initial configuration included a perfectly conducting disk (introduced via boundary conditions), threaded by a monopole magnetic field originating from a point below the disk. The domain was filled with constant magnetization plasma ($\beta = 1/9$) with pressure $p \propto z^{-4}$, density $\rho \propto z^{-3}$ and zero velocity. The central region of the disk was set to rotate with either the Keplerian or the solid body rotation law. As the simulation started, the central rotator launched a magnetically-driven collimated outflow. The jets were traced until their head reached a distance of about one thousand times the rotator radius. In the case of the solid body rotation, the kink mode instability seemed to being able to significantly disrupt the jet, whereas in the Keplerian case the jet has clearly preserved its integrity, though with noticeable structure generated near its axis. A similar setup using a Keplerian rotation law was studied with special relativistic high-resolution adaptive mesh refinement simulations by one of the authors (Porth, 2013). Although the simulations were not run for a very long time, they confirmed the stability of the jet launching region and the high resolution allowed to identify filamentary structure in the jets current distribution conducive to magnetic dissipation.

McKinney and Blandford (2009) used 3D relativistic MHD simulation to study the long-term stability of the jet produced in the context of the MRI-driven accretion onto a rotating black hole. Their initial configuration describes an equilibrium gas torus aligned with the rotational axis of the black hole and threaded with the purely poloidal magnetic field aligned with the isodensity surfaces of the torus. The exterior of the torus is unmagnetized and filled with tenuous gas whose mass density and pressure scale as $\rho \propto r^{-3/2}$ and $p \propto r^{-5/3}$, where r is the radial coordinate of the Kerr–Schild coordinates (when r is large, it is just the distance from the black hole). The emerging jet is approximately conical in shape. It is not destroyed by the kink mode, as one could expect from the Kruskal–Shafranov criterion, but reaches the outer boundary of the computational domain, located at $r = 10^3 r_g$, unscathed. Moreover, they claim that the perturbations do not grow beyond the level introduced by the turbulent accreting flow of the torus.

Porth and Komissarov (2015) used the 3D periodic box setup to study the stability of expanding relativistic jets with $\sigma \lesssim 1$ and predominantly azimuthal magnetic field. Within the box, their jets had cylindrical geometry and their expansion was promoted via a forced decline of the external gas pressure. The temporal rate of the decline was set to what would be seen in a reference frame moving with relativistic speed through the atmosphere with the gas pressure $p \propto r^{-a}$. The results showed progressively increasing reduction of the instability growth rate with increasing value of a, leading to its almost complete suppression for $a \geq 2$. Interestingly, the instability mostly affected the current-carrying core, which refused to expand at the same rate as the jet boundary. At low jet expansion rates (due to the slow decrease of the external pressure), where the core occupied a large fraction of the jet volume, its instability eventually disrupted the whole of the jet. At high expansion rates, it remained confined to the deep interior of the jet. The development of such a core in the process of magnetic jet acceleration was predicted theoretically (Bogovalov, 1995; Beskin and Nokhrina, 2009) and confirmed in computer simulations (Komissarov et al., 2009; Moll et al., 2008)

The growth rate of instabilities depends on the details of the jet internal structure as well, with some configurations offering slower growth rates or/and shorter range of unstable modes than others. Yet the jet expansion provides the most robust explanation to how the astrophysical jets manage to escape so far away from their engines without being destroyed by the instabilities.

The issue of stability is connected with the long established division of the extended extragalactic radio sources roughly into the two main morphological types in the Fanaroff–Riley classification (Fanaroff and Riley, 1974). The jets of powerful FR2 type sources remain coherent until they reach the remote parts of the extended radio lobes (normally tens or hundreds kpc away from the central source) where they produce bright hot spots, usually associated with the termination shocks of supersonic (super-fast-magnetosonic) jets. In contrast, the jets of weaker FR1 sources seem to terminate well before reaching the outer parts of their lobes, producing a less compact region of somewhat enhanced emission (a warm spot). In a fraction of FR1 sources, the jets do not look like structures inside the extended lobes at all. Instead, the lobes appear as a broader and more amorphous continuations of the jets, very much like the plumes produced by the initially supersonic jets of rocket engines. This similarity motivated the early analytical and numerical turbulent jet models of FR1 jets (Bicknell, 1984; Komissarov, 1990). Since this implies that these jets have been strongly affected by instabilities, one has to understand what has accelerated their growth in these jets at the high pc- or lower kpc-scales.

Falle (1991b) has shown that any initially free-expanding jet propagating though a cold gas with density $\rho \propto r^{-b}$ (where $b < 2$) eventually inflates a cocoon (aka radio lobe) around itself and is prevented from further expansion by the cocoon's thermal pressure. Moreover, the length of the quasi-cylindrical section which begins at the reconfinement point and ends at the termination shock increases in time (in agreement with their 2D simulations Falle, 1991b). Thus more space is given for the instabilities to grow (see Eqs. (23) and (26)). They argued that eventually the jet becomes turbulent, mixes with its cocoon and slows down to subsonic speeds, and that this constitutes the transition from the FR2 to the FR1 morphology. Recent 3D hydrodynamic simulations by Massaglia and collaborators (Massaglia et al., 2016) and MHD (Massaglia et al., 2019) simulations of non-relativistic cylindrical jets provided the first demonstration of such a transition. In the simulations they tried to reproduce the conditions of X-ray coronas of massive elliptical galaxies and found that jets of lower power (corresponding to FR1 sources) become fully turbulent and do no longer produce a leading hot spot on the kpc scales, as observed. Fig. 6 shows an exemplary non-relativistic MHD simulation of jet propagation targeted at reproducing FR1 type jets from their study (Massaglia et al., 2019). In this case, the jet is swept back by a galactic wind with $v \sim 100$ km s^{-1} producing a wide-angle-tail morphology as observed for example in the radio galaxy 3C 465.

The only issue with these models is that the jets are injected into the computational domain not as freely expanding flows but as perfectly collimated cylindrical flows with more or less arbitrary parameters. This may seem a minor issue, however, the jet parameters after the reconfinement point are not arbitrary but dictated by the reconfinement process (Falle, 1991b; Komissarov and Falle, 1998). For example, the jet Mach number after the reconfinement is determined by its initial opening angle and the jet radius by the cocoon pressure that drives the reconfinement. In contrast, an arbitrarily set cylindrical jet of the same power can end up being (1) under-expanded and pinch its way through the external gas with ease, or (2) over-expanded, in which case it gets immediately crushed by the pressure of the cocoon it inflates. The usual practice of setting the jet pressure equal to the undisturbed external gas does not help as in the cylindrical jet emerging inside the cocoon after the reconfinement, the jet pressure is matched to the cocoon pressure which can be much higher.

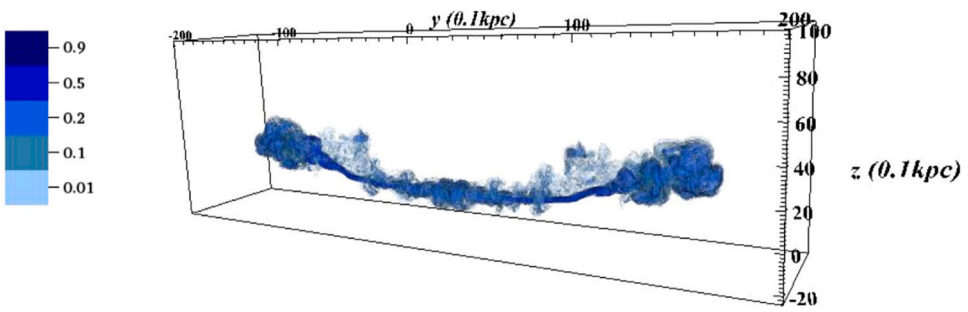

Fig. 6. Three-dimensional iso-contours of a scalar tracer distribution for a magnetohydrodynamic simulation of a wide-angle-tail FR1 jet, with plasma-β of 3, 4.8×10^7 yrs after jet injection. The size of the computational box is $12.4\times20\times8$ kpc.
Source: From Massaglia et al. (2019).

Tchekhovskoy and Bromberg (2016) carried out relativistic 3D MHD simulations which were similar in their setup to those by Moll et al. (2008) but like (Massaglia et al., 2016) were aimed at the jet propagation through the X-ray coronas of giant elliptical galaxies. To this end they introduced a perfectly conducting rotating sphere of the radius $r_{in} = 100$ pc. Its angular velocity was such that the light cylinder radius $r_{LC} = 1.25r_{in}$. The sphere was surrounded by a cold gas of density (a) $\rho \propto r^{-1}$ or (2) $\rho \propto r^{-1}$ for $r < 10$ kpc and $\rho \propto r^{-2.5}$ for $r > 10$ kpc. The configuration was steady-state as the gravity was ignored. The whole domain was threaded with a monopole magnetic field. Like in Moll et al. (2008), the rotation leads to a magnetically-driven outflow. The initial relativistic magnetization parameter of the outflow $\sigma_0 = 25$ and at the fast magnetosonic point the Lorentz factor of its bulk motion is expected to be $\gamma_f \approx \sigma_0^{1/3} \approx 3$ (see Beskin et al., 1998). However, in the simulations the Lorentz factor remains of the "order unity" and hence the flow never becomes super-fast-magnetosonic. Thus, the outflows generated in the simulations are not proper jets but rather magnetic towers, which are produced in a somewhat different geometry compared to the original model by Lynden-Bell (2003). They are confined by the thermal pressure of the shocked external gas and their faster expansion along the rotational axis is determined by the high axial pressure of the z-pinch. The detailed dynamics of such outflows is described in the earlier studies of jets in the context of GRB research (Komissarov et al., 2007; Bromberg and Tchekhovskoy, 2016). Although not able to capture the properties of AGN jets on kpc scales, the study demonstrates that even if the magnetic field can inhibit the KHI modes, the CD-instabilities take over and can disrupt the jets when the final quasi-cylindrical section becomes sufficiently long, leading to a qualitative change in the large scale morphology of the lobes they inflate.

Yet another potentially disruptive jet instability is encountered in differentially rotating two-component jets which can give rise to a relativistic variant of the well known Rayleigh-instability of rotating fluids. This was studied by Meliani and Keppens (2007, 2009) and recently by Millas et al. (2017) who extended this study to magnetized jets. While dynamically important close to the central engine, the rotation is expected to be too weak at the kpc-scales where the AGN jets become reconfined.

The theory of magnetically-accelerated steady-state axisymmetric relativistic jets shows that their asymptotic magnetization remains sufficiently high with $\sigma \lesssim 1$ (Lyubarsky, 2010; Komissarov et al., 2009). The 2D axisymmetric simulations of such jets drilling through a uniform external medium show that they produce conspicuous nose cones (Komissarov, 1999b). Such structures are not present in the large-scale structure of FR2 radio sources, in apparent conflict with the theory. However, 3D simulations of such jets (Mignone et al., 2010) show that this structure is unstable, becomes disrupted and swept back into the jet cocoon by the ram pressure of the external gas.

Gourgouliatos and Komissarov (2018a) studied the reconfinement of hypersonic AGN jets by the thermal pressure of the X-ray galactic coronas using 3D hydrodynamic simulations. For the FR1 jets, such a reconfinement is expected within the first few kiloparsecs and hence still inside the dense core of the X-ray gas (Porth and Komissarov, 2015). Quite unexpectedly, they found a rapid transition to fully turbulent flow right at the reconfinement point. A similar phenomenon was seen in their simulations of the jet reconfinement by a low-density constant-pressure external gas and in the 3D simulations of FR2 jets by Matsumoto and Masada (2019). A closer look revealed that the culprit was the centrifugal instability associated with the curved streamlines of the flow downstream of the reconfinement shock (Matsumoto and Masada, 2013; Gourgouliatos and Komissarov, 2018b). Its non-linear phase is illustrated in Fig. 7.

The non-axisymmetric nature of the instability explains why it was not seen in the earlier 2D simulations of jets undergoing reconfinement by the external pressure. The centrifugal instability can be suppressed by a relatively weak azimuthal magnetic field and develops only in kinetic-energy-dominated jets (Komissarov et al., 2019), which can be used for the physical diagnostic of jets.

Apart from advancing our understanding of the jet dynamics, these and many other recent studies have shown that the 3D geometry is paramount in simulations of jets, particularly when strong magnetic fields are involved. Not only theoretical axisymmetric models but also steady-state and time-dependent axisymmetric numerical simulations are drastically altered by the third degree of freedom.

3.6. Jet's impact on the parent galaxies

3.6.1. Interaction with the cooling flows

There are a number of interesting and important astrophysical problems that are concerned not with the physics of the astrophysical jets themselves but rather with the impact they can make on their surroundings. One such problem involves the dynamics of hot gas in massive elliptic galaxies and clusters of galaxies. The radiative cooling times of the gas is shorter than their life-time and the loss of pressure support in the central core of their distribution due to this cooling is expected to drive a subsonic inflow towards the center of the massive central galaxy. This cooled gas would form clouds and give birth to young stars, making these central galaxies much bluer and brighter than they actually are (Fabian, 1994). One possible solution to this conundrum is heating of the accreting gas by the AGN. Since this cooling gas may actually be the main channel of the "fuel" supply to the AGN, this leads to an interesting self-regulation problem. As the galaxies and clusters form via the same type of flows in the early Universe, this issue gets a cosmological dimension as well.

The AGN can heat and slow down the cooling flow via an inverse-Compton scattering of the AGN hard radiation. However, this is unlikely to be the case as the optical depth of the cooling flows remains below unity down to the distance $r = 100$ pc from the AGN (Omma et al., 2004). The second possibility is mechanical heating by the AGN jets (or winds) and it is supported by the observations of X-ray

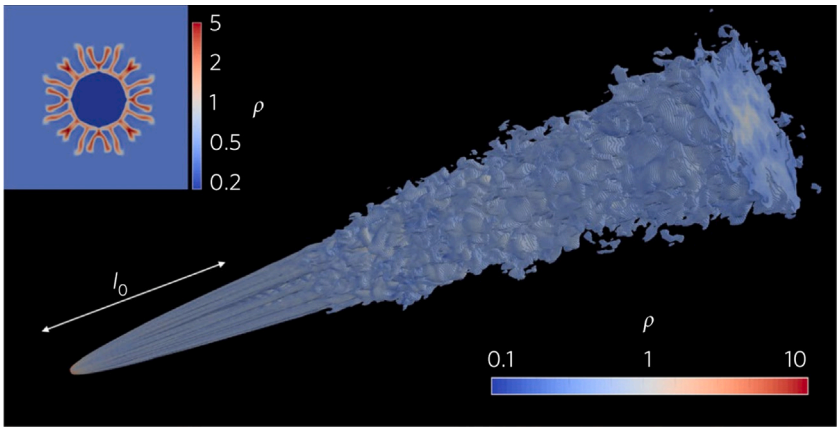

Fig. 7. Development of the centrifugal instability in reconfining jets, from Gourgouliatos and Komissarov (2018a). Due to the curved-streamlines, fluid at the contact discontinuity experiences an outwardly accelerating force giving rise to a Rayleigh–Taylor finger-like appearance of the instability (best seen in the cross-jet inset) which promotes strong mixing with the ambient material.

"cavities" in the central parts of galactic clusters, that are blown out by the radio jets. The heating by jets can occur via many different channels. First, the cooling flow can be heated by the shocks driven into the it by the jets (or winds). Second, the jets can push the central dense and cooler gas of the cooling flow out, where it will mix with hotter parts of the flow. Third, the gas of the cooling flow can turbulently mix with the extremely hot gas of the jet cocoon. The jets can excite the large-scale gravitational oscillations or meridional circulation of the cooling flow, which heat the gas when their kinetic energy is dissipated. High energy cosmic rays may also provide a substantial contribution to the heating.

A number of studies tried to address the jet heating issue via numerical simulations (Quilis et al., 2001; Reynolds et al., 2002; Brüggen and Kaiser, 2002; Omma et al., 2004; Zanni et al., 2005; Vernaleo and Reynolds, 2007; Cattaneo and Teyssier, 2007; Brüggen et al., 2007, 2009; O'Neill and Jones, 2010; Perucho et al., 2011, 2014; Weinberger et al., 2017; Ruszkowski et al., 2017). The problem is quite challenging as it involves multi-phase gas, processes on different spatial and time scales, radiative cooling, thermal conduction, magnetic field and turbulence. The direct mechanical impact of the jet on the cluster gas depends on its ability to create a thick over-pressured cocoon, which drives strong shocks into the surrounding gas, thus displacing it not only in the jet direction but also perpendicular to it. In the numerical simulations, this strongly depends on the simulation setup. For example, if one sets up a perfectly collimated supersonic jet of a given thrust, then its initial advance speed is determined not only by the density of the external gas but also by the initial jet radius. Set the radius too small and the jet will pinch through the gas like a needle, only weakly disturbing it. Set it too large and the jet will be crushed by the pressure of its own cocoon, resulting in a hot bubble driving a quasi-spherical shock through the external gas. In the case of AGN jets, their radius at a given distance from the central engine is determined by the interaction with their environment prior to reaching this distance. In the cooling flow simulations, it is set rather arbitrarily and is often dictated by the computational constraints rather than by the jet physics.

Most of the simulations thus far were Newtonian. In fact, high-speed jets present a computational challenge as the Courant–Friedrichs–Lewy stability condition sets a small time step. Combined with the large global time-scale of the problem this implies an uncomfortably long CPU time. For this reason, the jet speed is usually set to a value which is significantly below the speed of light. This however, reduces the jet ability to inflate an extensive cocoon by the effective decrease of the cocoon pressure relative to the ram pressure of the jet. For example, by setting the jet speed to 10^4 km/s, the thermal energy supplied by the jet to the cocoon of a given length is reduced compared to the relativistic jet of the same thrust by the factor of sixty (see Eq. (20)), implying almost eight times smaller cocoon radius. This may explain why in many such simulations the large-scale effect of the jet is limited to a sufficiently narrow region near the jet axis (e.g. Vernaleo and Reynolds, 2006; Martizzi et al., 2019). As a way out of this problem, a very wide-opening-angle AGN outflows (e.g. more like winds than the collimated radio jets, e.g. Prasad et al., 2015; Hillel and Soker, 2017) and wobbly or precessing jets were considered (e.g. Heinz et al., 2006; Gaspari et al., 2012; Bourne and Sijacki, 2017; Martizzi et al., 2019). In both cases, the idea is to spread the jet thrust over larger area and hence to reduce the advance speed of its head. This leads to a more rounded cocoon and a more isotropic heating of the cluster gas. The recent experiments with relativistic jets have confirmed that they are significantly more efficient heaters of the cluster gas by means of the cocoon driven shocks (Perucho et al., 2011, 2014).

In order to study the long term effects, the simulations have to be optimized by reducing the numerical resolution down to only several cells across the jet radius. Such a low resolution means that the jet dynamics cannot be reproduced adequately and this is likely to have severe implications for the problem of its cocoon interaction with the cooling flow. This is because the advance speed of the cocoon in the jet direction depends on the area over which the jet thrust is spread out near the jet head. This spreading is dictated by jet interaction with the cocoon, via the reconfinement shock, jet instabilities leading to the jet wobbling (the so-called "dentist drill" behavior) etc. Summarizing, we agree with the conclusion made by Martizzi et al. (2019) that although the simulations have provided useful guidelines to the problem, no firm conclusions of the efficiency of the jet heating of the cooling flows can be drawn at the moment.

3.6.2. *Interaction with clumpy ISM*

While in the local Universe the gas component of the host elliptical galaxies is dominated by a rather tenuous and hot X-ray emitting component, at high redshift there is more gas and a significant fraction of it is in the form of warm and cold clouds. The parent galaxies of low redshift radio sources can also get a significant optical-line-emitting gas component via a relatively recent merger with a gas-rich galaxy. Moreover, such clouds are a natural product of cooling flows.

Massive clouds can present a formidable obstacle for newly born jets. Their interaction with such clouds can be highly disruptive for the jet, promoting rapid release of its energy relatively close to the AGN. The released energy can have a strong effect on the ISM of the parent galaxy by removing the hot component and dispersing some clouds, thus temporarily suppressing the star formation. On the other hand the increased surrounding pressure may trigger gravitational collapse of the clouds, thus promoting the star formation.

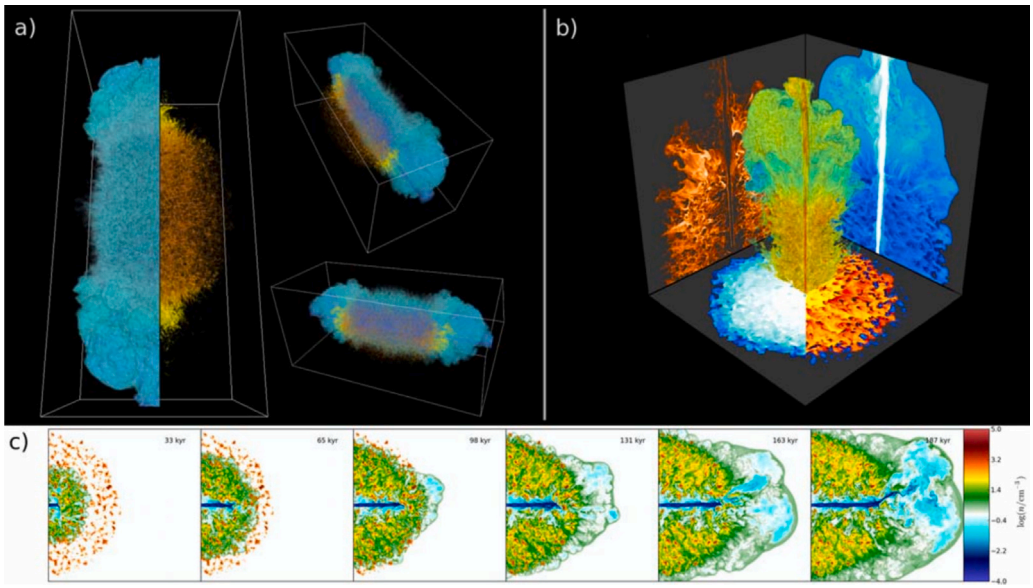

Fig. 8. Three-dimensional relativistic hydrodynamic simulations of AGN jets interacting with the ISM of a forming galaxy from Wagner et al. (2016). (a) Volume rendering at various angles of the jet (blue) and the dispersed clouds in orange. (b) Volume render of the jet plasma (central column), and projections of mid-plane slices of various physical quantities to the box faces. Back-left: kinetic energy of clouds, back-right: velocity map, bottom-left: thermal pressure map, bottom-right: temperature map. (c) Mid-plane slices of the density showing the evolution of the jet through the two-phase ISM. (For interpretation of the references to color in this figure legend, the reader is referred to the web version of this article.)

The first computer simulations of the jet interaction with the ISM clouds were carried out in slab geometry (e.g. Bicknell et al., 2003; Antonuccio-Delogu and Silk, 2008). Although this geometry has some advantages compared to the axisymmetry and allows to study some aspects of the jet-cloud interaction, the problem is inherently three-dimensional. The first 3D hydrodynamic simulations of the type carried out by Sutherland and Bicknell (2007) were focused on the physics of the young jets associated with compact steep spectrum sources (CSS). The initial distribution of warm (10^4 K) clouds was modeled as an almost Keplerian disk of $\approx$ 400 pc radius and $\approx$ 100 pc scale height. Their distribution was generated using a sophisticated statistical model adopted from the theory of turbulence, with the maximum size of the generated clouds of 25 pc. The space between the clouds was filled with hot gas of temperature 10^7 K. The simulations were run on a 512^3 grid with a 2 pc cell size using a Newtonian code. The jet was injected from a nozzle of 20 pc radius as a perfectly collimated cylindrical flow and was pressure-matched to the ISM. Its parameters were chosen to emulate a relativistic jet with Lorentz factor $\gamma = 5$ and kinetic power of 3×10^{43} erg s^{-1}, using the prescription given in Komissarov and Falle (1996). The simulations revealed four phases of the interaction with ISM, which persisted in later more advanced experiments. In the "flood and channel phase", the jet makes its initial advance though the disk, entraining and destroying clouds that happen to be on its way and getting more and more disrupted in the process. In the "bubble phase", the stifled jet inflates a quasi-spherical high-temperature and high-pressure bubble that grows in size faster than the jet and eventually engulfs the whole disk of clouds. This bubble is the same as the jet cocoon but it is heavily loaded with the entrained ISM material. It drives a strong bow shock that removes the hot component of ISM and a strong conical shock into the low pressure jet. During the "jet-breakout phase", the jet clears its path through the disk of clouds and begins to flow freely through it. Its head eventually catches up with the shock bubble. In the final "classic phase", the jet develops the large scale structure typical for jets propagating through a smooth non-clumpy environment, with its leading termination shock and backflow. Like in all other simulations where a perfectly collimated jet of a given radius is injected into the computational domain, here the results are inevitably influenced by the choice of this initial jet radius. In reality, the geometry of an AGN jet, including its radius at a given distance is strongly influenced by the conditions in its environment. For the problem at hand, these conditions are set by the violent interaction of the jet with ISM and hence the jet radius is subject to a complicated non-linear self-regulating process. Moreover, even assuming the relatively large jet half-opening angle $\theta_j = 0.1$, the distance from the AGN where the jet radius reaches the value of 20 pc, which is set as the initial radius in the simulations, is about 200 pc – well outside of the disk.

Later, a very similar study was carried out by Gaibler et al. (2011) but now with focus on the gas-rich high redshift galaxies. So their disk of clouds had the radial and vertical scales of 5 kpc and 1.5 kpc respectively. Its total mass was $1.5\times10^{11}\,M_\odot$. They used a Newtonian code with adaptive mesh (AMR) allowing the minimum cell size of 63 pc and the effective grid of 2048^3 cells. A bipolar perfectly collimated jet was released via a virtual orifice of 400 pc radius located in the center of the disk and aligned with the disk axis. The jet speed and power were set to 0.8 c and 5.5×10^{45}erg s^{-1} respectively. The evolution proceeded through the same phases as in Sutherland and Bicknell (2007) but with somewhat different timing for the two disk hemispheres due to lack of the reflection symmetry in the statistical realization of the cloud distribution. As a result, the large-scale structure produced by the jets was highly asymmetric. Later, the simulations were augmented with a subgrid model of star formation in order to understand whether the jet impact leads to its inhibition or promotion (Gaibler et al., 2012). It was found that up to $10^{10}\,M_\odot$ of additionally formed new stars can be produced in one cycle of AGN activity. The main region of the star formation was located in a ring shaped volume of the disk surrounding the central "hole" made in the disk by the jet.

The study was continued by Wagner and Bicknell (2011), Wagner et al. (2012) using a relativistic code. They build a suite of 29 numerical experiments, aimed to explore the dependence of AGN feedback efficiency of the jet and ISM parameters. The warm clouds were distributed uniformly within a sphere of the 0.5 kpc radius. The computational domain had a size of 1 kpc^3 with the center of the cloud distribution (and the jet inlet) placed in the middle of one of its faces. The AMR grid had the effective resolution of 512^3 or 1024^3, with the minimum cell size of 1 or 2 pc. The initial jet radius was 20 pc and the maximum cloud radii varied from 10 to 50 parsec depending on the run. The results of these and some previous simulations were also summarized in Wagner et al. (2016) and we reproduce one of their figures in Fig. 8. They

show that in the bubble phase the bubble-driven shock sweeps away the hot-phase gas but disturbs the clouds only slightly. However the clouds are strongly effected by the fast streams of shocked jet plasma escaping from the high pressure impact sites in the jet through the space between the clouds in all directions. The speed of the streams could be as high as c/3 and provided sufficient ram pressure to expel the clouds from the jet surrounding. In the process, the clouds were mechanically ablated by the streams. The smaller clouds were predominantly dispersed and ablated whereas the larger clouds survived and were found more susceptible to the collapse induced by the increased pressure inside the bubble. The critical size is found to be about 25 pc. The overall outcome of the jet feedback was found to be sensitive to the geometry of the clouds distribution. For a disk-like distribution, the destructive role of the jet was limited and the star-formation rate could be significantly increased. For a spherical distribution, the jet would be stuck inside it for longer and the streams of the shocked jet plasma had more time to ablate, disperse and accelerate the clouds. Obviously, the jet effectiveness in destroying the clouds and suppressing the star formation depended on the jet kinetic power, which was quantified in terms of the parameter $\eta = L_{jet}/L_{edd}$. The critical value was estimated at $\eta_{cr} \approx 10^{-4}$.

These simulations look very impressive, producing complex structures which have the sweet flavor of reality about them. However, the clouds are not well resolved and the process of their mechanical ablation and destruction is definitely not captured properly. The Rayleigh–Tailor and Kelvin–Helmholtz instabilities should create turbulent mixing layers between the clouds and the surrounding flow of the shocked jet plasma which determine the rates of mixing, heating and mass-loading. Such layers are not captured and the rates seen in the simulations are dictated by the diffusion properties of the utilized numerical schemes rather than by the actual physics of the interaction (Pittard et al., 2009). Just like in the case of jet interactions with cooling flows, the current state-of-art simulations of the AGN feedback via radio jets provide useful guidelines but do not allow to draw firm conclusions yet.

4. Coming of age

As an area of research, the computer simulations of jets are entering a new phase, which may be described as maturity.

For a long time, this type of research required very high coding skills as the researcher would have to be able to make significant changes to the available code, if not writing it from scratch. Most "home-made" codes were not particularly user-friendly as the developers did not think that their codes would be modified by someone but themselves and their close collaborators. Specialist knowledge of computers and their infrastructure was also required. The researchers had to be highly proficient in the numerical methods too. Once all these prerequisites were met, there was also the little issue of becoming an expert in astrophysics as well.

With the advance of publicly available codes like `Athena(++)` (Stone et al., 2020), `FLASH` (Fryxell et al., 2000), `Pluto` (Mignone et al., 2007), `Ramses` (Teyssier, 2002) or `MPI-AMRVAC`, co-developed by one of the authors (Keppens et al., 2012; Porth et al., 2014; Xia et al., 2018) (and its general relativistic framework `BHAC` (Porth et al., 2017)), the situation has changed. Although a basic understanding of the algorithms is still required, the demand to be proficient in all the nitty-gritty of the simulations has subsided. This is just like driving a car does not require much knowledge of how its engine works. A much wider scientific community can now run computer simulations and research students are routinely trained in this regard. This and the availability of quite powerful supercomputers in even second-tier research centers (unthinkable even twenty years ago) are the two main reasons why the computer simulations in astrophysics in general and in the physics of astrophysical jets in particular are entering a qualitatively different new phase.

As we have discussed here, a number of fundamental questions in the jet dynamics appear to have been resolved via a combination of theoretical analysis and computer simulations during the last two decades. There are however other issues where the progress has been rather slow and its acceleration will require significant efforts.

One key unsolved issue of relativistic jets is the nature of their composition (e.g. the recent review by Blandford et al., 2019). At first sight, it seems surprising that given the wealth of detail recovered by modern computer simulations, the question whether an AGN jet is primarily composed of lepton pairs or hadrons (baryons and mesons) could not yet conclusively be answered. This comes about as within the single-fluid model, the plasma composition does not influence the dynamics, only the emission properties. Since hadronic emission is generally less radiatively efficient, the models of hadronic high-energy emission require (unrealistically) high jet energies if they are to match the double-humped spectral energy distribution. Observations of neutrino emission from blazar sources such as TXS 506+056 as indicated by the IceCube experiment (Aartsen et al., 2018) however require at least some hadronic component to be present in the jet. This issue is coined the "energy crisis" of AGN jets (Sikora et al., 2009; Zdziarski and Bottcher, 2015; Liodakis and Petropoulou, 2020).

Whether the baryonic matter is part of the jet from the start or whether it is "mixed" in via a range of fluid instabilities is not yet clear. Numerical simulations of mixing and entrainment (e.g. Walg et al.; Chatterjee et al., 2019) will play a part in modeling the "loading" of jets, hopefully leading to a resolution of the jet composition issue.

Another major issue in understanding astrophysical jets concerns the origin of non-thermal emission. The fluid description employed in state-of-the-art studies provides only the integral characteristics of plasma, such as the total number density of particles, their mean energy and the magnetic field strength. This is not sufficient for the emission calculations which require the energy–momentum distribution of the non-thermal component. Hence to address the jet emission, we need to go beyond the fluid description.

One may introduce the spectrum of the non-thermal component in a parametric form with few parameters whose evolution is tied to the background fluid flow. In the crudest example, one can assume that the non-thermal energy spectrum is a power law with given power index and energy range and demand that the non-thermal energy density is a fixed fraction of the internal energy density of the fluid model. However, this is just a fancy way of visualizing the fluid solution (see e.g. the attempts by one of the authors Porth et al., 2011), whereas a proper model should address the issues of the acceleration, transport and radiation losses with some rigor.

Several schemes for particle transport, heating and acceleration in jets have been introduced in recent years, either based on Lagrangian tracer particles or on additional fluid tracers (Ressler et al., 2015; Chael et al., 2017; Vaidya et al., 2018; Ohmura et al., 2020). The most difficult mechanism to account for is particle acceleration, which can occur at shocks, at sites of magnetic reconnection and in regions of developed turbulence. Shock acceleration has traditionally been the most popular mechanism, however the recent studies show that in relativistic plasma it is not an efficient mechanism. At least, it is not captured in the dedicated PIC-simulations of relativistic magnetized shocks. This is in contrast to relativistic magnetic reconnection, where the PIC simulations find that the non-thermal particle acceleration is very efficient.

The main problem is that the particle acceleration is a microphysical process which occurs on much smaller scales than the jet flow, unless we are interested only in the ultra-high energy particles with macroscopic Larmor radius. Collimated particle beams can be studied using the PIC approach (e.g. Nishikawa et al., 2016; Alves et al., 2018, 2019) but when the structures emerging in such studies are driven by the kinetic processes, we are dealing with scales that are much smaller than what is resolved in astronomical observations of jets.

We can see two ways of how the particle acceleration can be incorporated into the fluid models of jets. One is the development of hybrid fluid–kinetic codes, where most of the jet dynamics is described using the fluid model and in few sites of special interest it is done via the kinetic model (likely using the PIC methodology). The fluid model has to be complemented with the facilities responsible for the transport of non-thermal particles, which describes how the particle spectrum evolves while been transported by the flow from one acceleration site to another. For this approach to work, there have to be a small number of acceleration sites as they would have to be treated with very high numerical resolution. In the context of solar- and space-physics, two-way fluid–kinetic couplings have already been demonstrated successfully (Daldorff et al., 2014; Makwana et al., 2017). These hybrid schemes are now applied to global scenarios where PIC domains focus on the current-sheets arising in sun–planet (Chen et al.) or planet–moon magnetospheric interactions (Tóth et al., 2016).

The second approach is the development of subgrid models of particle acceleration. For this to work, the particle acceleration has to be well understood and reduced to reasonably accurate and sufficiently simple analytic or at least semi-analytic representations. As far as the magnetic reconnection is concerned, we have not yet reached this stage, although first tentative steps into this direction have been made (e.g. Ball et al., 2018; Davelaar et al., 2019).

Another issue is related to the fact that the available RMHD codes cannot handle the high magnetization regime where $\sigma \gg 1$ and the RMHD equations become "stiff". As in this regime the plasma contributions to the total mass-energy and momentum are small and hence increasingly sensitive to the numerical errors, high accuracy and hence numerical resolution is needed even in smooth regions just to avoid the code crashing. As we have discussed earlier, such highly magnetized regions naturally develop near black holes due to the double-wind structure of flows powered by the Blandford–Znajek mechanism (similarly, high magnetization is expected in the magnetospheres of neutron stars). In the simulations, these regions are handled via artificial mass injection, which prevents otherwise inevitable code crash. On the other hand, the moderate bulk-motion Lorentz factors of AGN jets indicate the operation of some efficient physical process of mass-loading. Identification and studying of this process in future computer simulations require codes that can handle the high magnetization regime, perhaps by coupling to the set of force-free equations where appropriate (e.g. Lehner et al., 2012; Paschalidis and Shapiro, 2013).

4.1. Computing aspects

It has become quite clear that a comprehensive representation of the astrophysical jet dynamics and the jet interaction with its surrounding requires 3D simulations. The computational cost of explicit 3D integration (e.g. the CPU time) grows at least as n^4, where n is the number of grid-points in one direction. This is a very steep rise indeed. For example, if we need to increase the resolution by a factor of two and still complete the simulation within the same, usually already quite a long time, the number of processor cores would have to be increased a factor of sixteen. This means a much better and hence a much more expensive computer facility. So far the power of supercomputers was growing very fast, doubling every two years (the so-called Moore's law), which was mostly based on the ability to produce smaller and smaller transistors. However, the miniaturization trend is coming to an end as the size of the transistors is approaching the atomic scale where the limiting quantum effects become overwhelming. Another related problem is the increasing circuit energy loss and heating, limiting the microprocessor clock speed. Unless a radically new technological solution is found, the growth of available computer power will slow down significantly already within the decade (e.g. Waldrop, 2016).

Traditionally, astrophysical and fluid-dynamical applications have directly benefitted from developments in high-performance computing. This is because these applications are highly parallel and scale well to entire compute clusters. While the mean power of supercomputers available for astrophysical research is likely to grow faster than the top tier clusters (because of the current gap between them and the world leading machines), we do not expect the typical 3D simulations to go much beyond the 1000^3 grid for the next decade. We can see two trends: on the one hand, codes are more easy to handle for the user and faster general purpose clusters will become available to the astro community. This would allow more people to do simulations of the 1000^3 resolutions class. At the same time, to keep up with the growing demand on performance (with new compute-hungry applications such as machine learning entering the arena), engineers are forced to add more hierarchy, use accelerators like GPUs, and try to squeeze out performance on the lowest abstraction level as in vectorization (see for example the ARM Scalable Vector Extensions). Programming close to the particular hardware will be required for the physicist who wants to optimally benefit from the alluring performance gains that zetta-scale promises (a zetta-scale supercomputer performs 10^{21} floating point operations per second, three orders of magnitude more than what is within reach at the time of writing of this review). Hence once again, specialist knowledge will be required and it might be too much to bear for the astrophysical community alone. Fruitful collaboration between performance engineers and astrophysicists will be essential to bring numerical simulations of astrophysical phenomena to the next level.

Though even when fully harnessing zetta-scale which might become available in the late 2030s (see Liao et al., 2018, for a performance engineering perspective), the n^4 complexity means that going from exa- to zetta-scale by brute force would only yield an increase of linear resolution by a factor of less than six. This obviously puts not much of a dent in some very challenging global problems, for example the launching and afterglow of GRBs which are separated by ten orders or magnitude. The increased dynamic range however does allow to more carefully investigate convergence and increase the confidence of the numerical solutions.

Adaptive meshes may improve local resolution, but only if the volume covered by the finest mesh is only a small fraction of the computational domain. We are somewhat skeptical that novel algorithms for fluid dynamics will suddenly emerge and change the game as was the case with the invention of conservative shock-capturing schemes by Godunov (1959). For example, the methods being employed in production codes today are all based on schemes developed in the 1960s/1970s, with the discontinuous Galerkin methods being the most recent development dating back to 1973 (Reed and Hill, 1973).

The current hardware developments such as GPUs and manycore (vectorized) processors mean that there is an abundance of compute capability but limited memory bandwidth. This trend has increased over the years meaning that there is some pressure to "do more with the data", as in higher-order accurate methods (e.g. Felker and Stone, 2018; Most et al., 2019). In particular as the energy scales can be strongly disparate in jets (for example in regions of high magnetization, see above), high accuracy is required even in otherwise smooth parts of the jet flow (Tchekhovskoy et al., 2007). Transitioning from second- to fourth-order accurate schemes might hence be the most immediate way to improve simulations of astrophysical jets.

The limitations imposed by the computational facilities are likely to change the practice of computer simulations in several respects. The focus may switch from the direct simulations of large-scale problems which leave the local dynamics under-resolved, to high-resolution studies of the local processes. Clever algorithms where a lot of physics is included on the subgrid level may become much more widely used on the global scale.

When planning this review we opted to avoid simply listing relevant papers and decided to give more in-depth analysis of the progress achieved in a few important directions instead. The selection of papers inevitably reflects our subjective views and personal research interests. As a result, the review is not comprehensive and we issue our unreserved apology to the authors whose contributions have not made it into our bibliography.

We believe this review shows that the numerical studies of relativistic jets have grown up and matured: starting with first careful steps in the 1970s where the cocoon and bow-shock structure was established, over the childhood years marked by controversies over the Blandford–Znajek mechanism and relativistic jet self-collimation in the 1990s–2000s into the current era of large scale 3D simulations. While we remain humbled by the wealth of physical processes sampled by astrophysical jets, through numerical simulations we also have a powerful tool for their study at our disposal!

Acknowledgments

SK was supported via STFC Grant No. ST/N000676/1. We thank the anonymous referee for a careful reading of the manuscript and helpful suggestions that improved the presentation of this chapter.

References

IceCube Collaboration, Aartsen, M.G., Ackermann, M., et al., 2018. Science 361, eaat1378.
Abramowicz, M., Jaroszynski, M., Sikora, M., 1978. Astron. Astrophys. 63, 221.
Akiyama, K., Alberdi, A., et al., Event Horizon Telescope Collaboration, 2019. Astrophys. J. Lett. 875, L5.
Aloy, M.A., Müller, E., Ibáñez, J.M., Martí, J.M., MacFadyen, A., 2000. Astrophys. J. Lett. 531, L119.
Aloy, M.A., Rezzolla, L., 2006. Astrophys. J. Lett. 640, L115.
Alves, E.P., Zrake, J., Fiuza, F., 2018. Phys. Rev. Lett. 121, 245101.
Alves, E.P., Zrake, J., Fiuza, F., 2019. Phys. Plasmas 26, 072105.
Anile, A.M., Pennisi, S., 1987. Ann. H. P. Phys. Théorique 46, 27.
Antonuccio-Delogu, V., Silk, J., 2008. Mon. Not. R. Astron. Soc. 389, 1750.
Appl, S., Camenzind, M., 1992. Astron. Astrophys. 256, 354.
Appl, S., Camenzind, M., 1993. Astron. Astrophys. 270, 71.
Appl, S., Lery, T., Baty, H., 2000. Astron. Astrophys. 355, 818.
Balbus, S.A., Hawley, J.F., 1991. Astrophys. J. 376, 214.
Ball, D., Sironi, L., Özel, F., 2018. Astrophys. J. 862, 80.
Balsara, D.S., Spicer, D.S., 1999. J. Comput. Phys. 149, 270.
Baty, H., 2005. Astron. Astrophys. 430, 9.
Beckwith, K., Hawley, J.F., Krolik, J.H., 2008. Astrophys. J. 678, 1180.
Begelman, M.C., Blandford, R.D., Rees, M.J., 1984. Rev. Modern Phys. 56, 255.
Begelman, M.C., Li, Z., 1994. Astrophys. J. 426, 269.
Beskin, V.S., Kuznetsova, I.V., Rafikov, R.R., 1998. Mon. Not. R. Astron. Soc. 299, 341.
Beskin, V.S., Malyshkin, L.M., 2000. Astron. Lett. 26, 208.
Beskin, V.S., Nokhrina, E.E., 2009. Mon. Not. R. Astron. Soc. 397, 1486.
Bicknell, G.V., 1984. Astrophys. J. 286, 68.
Bicknell, G.V., Saxton, C.J., Sutherland, R.S., Midgley, S., Wagner, S.J., 2003. New A Rev. 47, 537.
Birkinshaw, M., 1991. The stability of jets. In: Hughes, P.A. (Ed.), Beams and Jets in Astrophysics, vol. 19. In: Cambridge Astrophysics Series, Cambridge University Press, Cambridge, UK, p. 278.
Bisnovatyi-Kogan, G.S., Ruzmaikin, A.A., 1976. Astrophys. Space Sci. 42, 401.
Blandford, R., Meier, D., Readhead, A., 2019. Annu. Rev. Astron. Astrophys. 57, 467.
Blandford, R.D., Payne, D.G., 1982. Mon. Not. R. Astron. Soc. 199, 883.
Blandford, R.D., Rees, M.J., 1974. Mon. Not. R. Astron. Soc. 169, 395.
Blandford, R.D., Znajek, R.L., 1977. Mon. Not. R. Astron. Soc. 179, 433.
Bodo, G., Cattaneo, F., Mignone, A., Rossi, P., 2014. Astrophys. J. Lett. 787, L13.
Bodo, G., Massaglia, S., Ferrari, A., Trussoni, E., 1994. Astron. Astrophys. 283, 655.
Bodo, G., Mignone, A., Rosner, R., 2004. Phys. Rev. E 70, 036304.
Bogovalov, S.V., 1995. Astron. Lett. 21, 565.
Bogovalov, S.V., 2001. Astron. Astrophys. 371, 1155.
Bourne, M.A., Sijacki, D., 2017. Mon. Not. R. Astron. Soc. 472, 4707.
Bromberg, O., Tchekhovskoy, A., 2016. Mon. Not. R. Astron. Soc. 456, 1739.
Brüggen, M., Heinz, S., Roediger, E., Ruszkowski, M., Simionescu, A., 2007. Mon. Not. R. Astron. Soc. 380, L67.
Brüggen, M., Kaiser, C.R., 2002. Nature 418, 301.
Brüggen, M., Scannapieco, E., Heinz, S., 2009. Mon. Not. R. Astron. Soc. 395, 2210.
Bugli, M., Del Zanna, L., Bucciantini, N., 2014. Mon. Not. R. Astron. Soc. 440, L41.
Camenzind, M., 1987. Astron. Astrophys. 184, 341.
Casse, F., Keppens, R., 2002. Astrophys. J. 581, 988.
Casse, F., Keppens, R., 2004. Astrophys. J. 601, 90.
Cattaneo, A., Teyssier, R., 2007. Mon. Not. R. Astron. Soc. 376, 1547.
Chael, A.A., Narayan, R., Sadowski, A., 2017. Mon. Not. R. Astron. Soc. 470, 2367.
Chatterjee, K., Liska, M., Tchekhovskoy, A., Markoff, S.B., 2019. Mon. Not. R. Astron. Soc. 490, 2200.
Chen, Y., Toth, G., Jia, X., et al., 2019, arXiv e-prints.
Chiueh, T., Li, Z.-Y., Begelman, M.C., 1991. Astrophys. J. 377, 462.
Clarke, D.A., Norman, M.L., Burns, J.O., 1986. Astrophys. J. Lett. 311, L63.
Contopoulos, I., Kazanas, D., 2002. Astrophys. J. 566, 336.
Copeland, J., 2006. The Secrets of Bletchley Park's Codebreaking Computers. Oxford University Press, Oxford.
Copeland, B.J., 2017. The Stanford Encyclopedia of Philosophy, winter 2017 ed. Metaphysics Research Lab, Stanford University,
Curtis, H., 1918. Pub. Lick. Obs 13, 31.
Daldorff, L.K.S., Tóth, G., Gombosi, T.I., et al., 2014. J. Comput. Phys. 268, 236.
Davelaar, J., Olivares, H., Porth, O., et al., 2019. Astron. Astrophys. 632, A2.
De Villiers, J.-P., 2006. Astrophysics arXiv e-prints.
De Villiers, J.-P., Hawley, J.F., Krolik, J.H., 2003. Astrophys. J. 599, 1238.
De Villiers, J.-P., Hawley, J.F., Krolik, J.H., Hirose, S., 2005. Astrophys. J. 620, 878.
Dedner, A., Kemm, F., Kröner, D., et al., 2002. J. Comput. Phys. 175, 645.
Del Zanna, L., Zanotti, O., Bucciantini, N., Londrillo, P., 2007. Astron. Astrophys. 473, 11.
Duncan, G.C., Hughes, P.A., 1994. Astrophys. J. Lett. 436, L119+.
Eichler, D., 1993. Astrophys. J. 419, 111.
Eulderink, F., Mellema, G., 1994. Astron. Astrophys. 284, 654.
Evans, C.R., Hawley, J.F., 1988. Astrophys. J. 332, 659.
Fabian, A.C., 1994. Annu. Rev. Astron. Astrophys. 32, 277.
Falle, S.A.E.G., 1991a. Mon. Not. R. Astron. Soc. 250, 581.
Falle, S.A.E.G., 1991b. Mon. Not. R. Astron. Soc. 250, 581.
Falle, S.A.E.G., Komissarov, S.S., 1996. Mon. Not. R. Astron. Soc. 278, 586.
Falle, S.A.E.G., Wilson, M.J., 1985. Mon. Not. R. Astron. Soc. 216, 79.
Fanaroff, B.L., Riley, J.M., 1974. Mon. Not. R. Astron. Soc. 167, 31P.
Felker, K.G., Stone, J.M., 2018. J. Comput. Phys. 375, 1365.
Ferrari, A., 1998. Annu. Rev. Astron. Astrophys. 36, 539.
Ferreira, J., 1997. Astron. Astrophys. 319, 340.
Fishbone, L.G., Moncrief, V., 1976. Astrophys. J. 207, 962.
Font, J.A., 2008. Living Rev. Relativ. 11, 7.
Font, J.A., Ibanez, J.M., Marquina, A., Marti, J.M., 1994. Astron. Astrophys. 282, 304.
Fryxell, B., Olson, K., Ricker, P., et al., 2000. Astrophys. J. Suppl. 131, 273.
Gaibler, V., Khochfar, S., Krause, M., 2011. Mon. Not. R. Astron. Soc. 411, 155.
Gaibler, V., Khochfar, S., Krause, M., Silk, J., 2012. Mon. Not. R. Astron. Soc. 425, 438.
Gaspari, M., Ruszkowski, M., Sharma, P., 2012. Astrophys. J. 746, 94.
Gourgouliatos, K.N., Komissarov, S.S., 2018a. Nat. Astron. 2, 167.
Gourgouliatos, K.N., Komissarov, S.S., 2018b. Mon. Not. R. Astron. Soc. 475, L125.
Guan, X., Gammie, C.F., Simon, J.B., Johnson, B.M., 2009. Astrophys. J. 694, 1010.
Hardee, P.E., 1987a. Astrophys. J. 313, 607.
Hardee, P.E., 1987b. Astrophys. J. 318, 78.
Heinz, S., Brüggen, M., Young, A., Levesque, E., 2006. Mon. Not. R. Astron. Soc. 373, L65.
Heyvaerts, J., Norman, C., 1989. Astrophys. J. 347, 1055.
Heyvaerts, J., Norman, C., 2003. Astrophys. J. 596, 1240.
Hillel, S., Soker, N., 2017. Astrophys. J. 845, 91.
Igumenshchev, I.V., 2008. Astrophys. J. 677, 317.
Keppens, R., Meliani, Z., van Marle, A.J., Delmont, P., Vlasis, A., van der Holst, B., 2012. Journal of Computational Physics 231 (3), 718 – 744.
Koide, S., 2003. Phys. Rev. D 67, 104010.
Koide, S., Nishikawa, K.-I., Mutel, R.L., 1996. Astrophys. J. Lett. 463, L71.
Koide, S., Shibata, K., Kudoh, T., 1998. Astrophys. J. Lett. 495, L63+.
Koide, S., Shibata, K., Kudoh, T., 1999. Astrophys. J. 522, 727.
Koide, S., Shibata, K., Kudoh, T., Meier, D.L., 2002. Science 295, 1688.
Komissarov, S.S., 1990. Astrophys. Space Sci. 171, 105.
Komissarov, S.S., 1999a. Mon. Not. R. Astron. Soc. 303, 343.
Komissarov, S.S., 1999b. Mon. Not. R. Astron. Soc. 308, 1069.
Komissarov, S.S., 2001a. Mon. Not. R. Astron. Soc. 326, L41.
Komissarov, S.S., 2001b. In: Toro, E.F. (Ed.), Godunov Methods: Theory and Applications. Kluwer Academic/Plenum Publishers, New York, p. 519.
Komissarov, S.S., 2002. Mon. Not. R. Astron. Soc. 336, 759.
Komissarov, S.S., 2004a. Mon. Not. R. Astron. Soc. 350, 427.
Komissarov, S.S., 2004b. Mon. Not. R. Astron. Soc. 350, 1431.
Komissarov, S.S., 2005. Mon. Not. R. Astron. Soc. 359, 801.
Komissarov, S.S., 2009. J. Korean Phys. Soc. 54, 2503.
Komissarov, S.S., Barkov, M.V., Vlahakis, N., Königl, A., 2007. Mon. Not. R. Astron. Soc. 380, 51.
Komissarov, S.S., Falle, S.A.E.G., 1996. In: Hardee, P.E., Bridle, A.H., Zensus, J.A. (Eds.), Energy Transport in Radio Galaxies and Quasars. In: Astronomical Society of the Pacific Conference Series, vol. 100, p. 173.

Komissarov, S.S., Falle, S.A.E.G., 1998. Mon. Not. R. Astron. Soc. 297, 1087.
Komissarov, S.S., Gourgouliatos, K.N., Matsumoto, J., 2019. Mon. Not. R. Astron. Soc. 488, 4061.
Komissarov, S.S., Vlahakis, N., Königl, A., 2010. Mon. Not. R. Astron. Soc. 407, 17.
Komissarov, S.S., Vlahakis, N., Königl, A., Barkov, M.V., 2009. Mon. Not. R. Astron. Soc. 394, 1182.
Konigl, A., 1980. Phys. Fluids 23, 1083.
Kozlowski, M., Jaroszynski, M., Abramowicz, M.A., 1978. Astron. Astrophys. 63, 209.
Landau, L.D., Lifshitz, E.M., 1959. Fluid Mechanics. Pergamon Press.
Lehner, L., Palenzuela, C., Liebling, S.L., Thompson, C., Hanna, C., 2012. Phys. Rev. D 86, 104035.
Li, Z.-Y., 1995. Astrophys. J. 444, 848.
Liao, X.-k., Lu, K., Yang, C.-q., et al., 2018. Front. Inf. Technol. Electron. Eng. 19, 1236.
Lind, K.R., Payne, D.G., Meier, D.L., Bland ford, R.D., 1989. Astrophys. J. 344, 89.
Liodakis, I., Petropoulou, M., 2020. Astrophys. J. Lett. 893, L20.
Liska, M., Tchekhovskoy, A., Quataert, E., 2020. Mon. Not. R. Astron. Soc. 494, 3656.
Lynden-Bell, D., 2003. Mon. Not. R. Astron. Soc. 341, 1360.
Lyubarskij, Y.E., 1992. Sov. Astron. Lett. 18, 356.
Lyubarsky, Y., 2009. Astrophys. J. 698, 1570.
Lyubarsky, Y.E., 2010. Mon. Not. R. Astron. Soc. 402, 353.
Lyubarsky, Y., Eichler, D., 2001. Astrophys. J. 562, 494.
MacFadyen, A.I., Woosley, S.E., 1999. Astrophys. J. 524, 262.
Makwana, K., Keppens, R., Lapenta, G., 2017. Comput. Phys. Comm. 221, 81.
Marshall, M.D., Avara, M.J., McKinney, J.C., 2018. Mon. Not. R. Astron. Soc. 478, 1837.
Marti, J.M., Mueller, E., Ibanez, J.M., 1994. Astron. Astrophys. 281, L9.
Martí, J.M., Müller, E., 2015. Living Rev. Comput. Astrophys. 1, 3.
Martí, J.M., Müller, E., Font, J.A., Ibáñez, J.M.Z., Marquina, A., 1997. Astrophys. J. 479, 151.
Martizzi, D., Quataert, E., Faucher-Giguère, C.-A., Fielding, D., 2019. Mon. Not. R. Astron. Soc. 483, 2465.
Massaglia, S., Bodo, G., Rossi, P., Capetti, S., Mignone, A., 2016. Astron. Astrophys. 596, A12.
Massaglia, S., Bodo, G., Rossi, P., Capetti, S., Mignone, A., 2019. Astron. Astrophys. 621, A132.
Matsumoto, J., Masada, Y., 2013. Astrophys. J. Lett. 772, L1.
Matsumoto, J., Masada, Y., 2019. Mon. Not. R. Astron. Soc. 490, 4271.
McKinney, J.C., Blandford, R.D., 2009. Mon. Not. R. Astron. Soc. 394, L126.
McKinney, J.C., Gammie, C.F., 2004a. Astrophys. J. 611, 977.
McKinney, J.C., Gammie, C.F., 2004b. Astrophys. J. 611, 977.
McKinney, J.C., Tchekhovskoy, A., Blandford, R.D., 2012. Mon. Not. R. Astron. Soc. 423, 3083.
Meliani, Z., Keppens, R., 2007. Astron. Astrophys. 475, 785.
Meliani, Z., Keppens, R., 2009. Astrophys. J. 705, 1594.
Mignone, A., Bodo, G., Massaglia, S., et al., 2007. Astrophys. J. Suppl. 170, 228.
Mignone, A., Rossi, P., Bodo, G., Ferrari, A., Massaglia, S., 2010. Mon. Not. R. Astron. Soc. 402, 7.
Miles, J.W., 1957. Acoust. Soc. Am. J. 29, 226.
Millas, D., Keppens, R., Meliani, Z., 2017. Mon. Not. R. Astron. Soc. 470, 592.
Mizuno, Y., Hardee, P., Hartmann, D.H., Nishikawa, K.-I., Zhang, B., 2008. Astrophys. J. 672, 72.
Moll, R., Spruit, H.C., Obergaulinger, M., 2008. Astron. Astrophys. 492, 621.
Most, E.R., Papenfort, L.J., Rezzolla, L., 2019. Mon. Not. R. Astron. Soc. 490, 3588.
Murphy, G.C., Ferreira, J., Zanni, C., 2010. Astron. Astrophys. 512, A82+.
Narayan, R., Igumenshchev, I.V., Abramowicz, M.A., 2003. Publ. Astron. Soc. Japan 55, L69.
Narayan, R., Sadowski, A., Penna, R.F., Kulkarni, A.K., 2012. Mon. Not. R. Astron. Soc. 426, 3241.
Nishikawa, K.-I., Koide, S., Sakai, J.-i., et al., 1997. Astrophys. J. Lett. 483, L45.
Nishikawa, K.-I., Mizuno, Y., Niemiec, J., et al., 2016. Galaxies 4, 38.
Norman, M.L., Smarr, L., Smith, M.D., Wilson, J.R., 1981. Astrophys. J. 247, 52.
Norman, M.L., Winkler, K.H.A., 1986. In: Winkler, K.-H.A., Norman, M.L. (Eds.), NATO Advanced Science Institutes (ASI) Series C, vol. 188, p. 449.
Norman, M.L., Winkler, K.H.A., Smarr, L., Smith, M.D., 1982. Astron. Astrophys. 113, 285.
Ohmura, T., Machida, M., Nakamura, K., Kudoh, Y., Matsumoto, R., 2020. Mon. Not. R. Astron. Soc.
Okamoto, I., 2002. Astrophys. J. Lett. 573, L31.
Omma, H., Binney, J., Bryan, G., Slyz, A., 2004. Mon. Not. R. Astron. Soc. 348, 1105.
O'Neill, S.M., Jones, T.W., 2010. Astrophys. J. 710, 180.
Ouyed, R., Pudritz, R.E., 1997. Astrophys. J. 482, 712.
Parfrey, K., Philippov, A., Cerutti, B., 2019. Phys. Rev. Lett. 122, 035101.
Paschalidis, V., Shapiro, S.L., 2013. Phys. Rev. D 88, 104031.
Payne, D.G., Cohn, H., 1985. Astrophys. J. 291, 655.
Perucho, M., 2019. Galaxies 7, 70.
Perucho, M., Martí, J.M., Hanasz, M., 2004. Astron. Astrophys. 427, 431.
Perucho, M., Martí, J.M., Hanasz, M., 2005. Astron. Astrophys. 443, 863.
Perucho, M., Martí, J.-M., Quilis, V., Ricciardelli, E., 2014. Mon. Not. R. Astron. Soc. 445, 1462.
Perucho, M., Quilis, V., Martí, J.-M., 2011. Astrophys. J. 743, 42.
Piran, T., 2004. Rev. Modern Phys. 76, 1143.
Pittard, J.M., Falle, S.A.E.G., Hartquist, T.W., Dyson, J.E., 2009. Mon. Not. R. Astron. Soc. 394, 1351.
Porth, O., 2013. Mon. Not. R. Astron. Soc. 429, 2482.
Porth, O., Chatterjee, K., Narayan, R., et al., 2019. Astrophys. J. Suppl. 243, 26.
Porth, O., Fendt, C., 2010. Astrophys. J. 709, 1100.
Porth, O., Fendt, C., Meliani, Z., Vaidya, B., 2011. Astrophys. J. 737, 42.
Porth, O., Komissarov, S.S., 2015. Mon. Not. R. Astron. Soc. 452, 1089.
Porth, O., Olivares, H., Mizuno, Y., et al., 2017. Comput. Astrophys. Cosmol. 4, 1.
Porth, O., Xia, C., Hendrix, T., Moschou, S.P., Keppens, R., 2014. Astrophys. J. Suppl. 214, 4.
Prasad, D., Sharma, P., Babul, A., 2015. Astrophys. J. 811, 108.
Punsly, B., Coroniti, F.V., 1990. Astrophys. J. 350, 518.
van Putten, M.H.P.M., 1993. Astrophys. J. Lett. 408, L21.
Qian, Q., Fendt, C., Noble, S., Bugli, M., 2017. Astrophys. J. 834, 29.
Qian, Q., Fendt, C., Vourellis, C., 2018. Astrophys. J. 859, 28.
Quilis, V., Bower, R.G., Balogh, M.L., 2001. Mon. Not. R. Astron. Soc. 328, 1091.
Rayburn, D.R., 1977. Mon. Not. R. Astron. Soc. 179, 603.
Reed, W., Hill, T., 1973. Tech. Report LA-UR-73479, Los Alamos Scientific Laboratory.
Ressler, S.M., Tchekhovskoy, A., Quataert, E., Chandra, M., Gammie, C.F., 2015. Mon. Not. R. Astron. Soc. 454, 1848.
Reynolds, C.S., Heinz, S., Begelman, M.C., 2002. Mon. Not. R. Astron. Soc. 332, 271.
Ripperda, B., Bacchini, F., Porth, O., et al., 2019. Astrophys. J. Suppl. 244, 10.
Romero, G.E., Vila, G.S. (Eds.), 2014. Lecture Notes in Physics. In: Introduction to Black Hole Astrophysics, vol, 876, Berlin Springer Verlag.
Rosen, A., Hardee, P.E., 2000. Astrophys. J. 542, 750.
Rosen, A., Hughes, P.A., Duncan, G.C., Hardee, P.E., 1999. Astrophys. J. 516, 729.
Ruszkowski, M., Yang, H.Y.K., Reynolds, C.S., 2017. Astrophys. J. 844, 13.
Ryan, B.R., Gammie, C.F., Fromang, S., Kestener, P., 2017. Astrophys. J. 840, 6.
Sanders, R.H., 1983. Astrophys. J. 266, 73.
Scheuer, P.A.G., 1974. Mon. Not. R. Astron. Soc. 166, 513.
Sheikhnezami, S., Fendt, C., Porth, O., Vaidya, B., Ghanbari, J., 2012. Astrophys. J. 757, 65.
Sikora, M., Begelman, M.C., 2013. Astrophys. J. Lett. 764, L24.
Sikora, M., Stawarz, Ł., Moderski, R., Nalewajko, K., Madejski, G.M., 2009. Astrophys. J. 704, 38.
Stepanovs, D., Fendt, C., 2014. Astrophys. J. 793, 31.
Stepanovs, D., Fendt, C., 2016. Astrophys. J. 825, 14.
Stone, J.M., Tomida, K., White, C.J., Felker, K.G., 2020. Astrophys. J. Suppl. 249, 4.
Sutherland, R.S., Bicknell, G.V., 2007. Astrophys. J. Suppl. 173, 37.
Tchekhovskoy, A., Bromberg, O., 2016. Mon. Not. R. Astron. Soc. 461, L46.
Tchekhovskoy, A., McKinney, J.C., Narayan, R., 2007. Mon. Not. R. Astron. Soc. 379, 469.
Tchekhovskoy, A., McKinney, J.C., Narayan, R., 2009. Astrophys. J. 699, 1789.
Tchekhovskoy, A., McKinney, J.C., Narayan, R., 2012. J. Phys. Conf. Ser. 372, 012040.
Tchekhovskoy, A., Narayan, R., McKinney, J.C., 2010a. Astrophys. J. 711, 50.
Tchekhovskoy, A., Narayan, R., McKinney, J.C., 2010b. New A 15, 749.
Tchekhovskoy, A., Narayan, R., McKinney, J.C., 2011. Mon. Not. R. Astron. Soc. 418, L79.
Teyssier, R., 2002. Astron. Astrophys. 385, 337.
Tomimatsu, A., 1994. Publ. Astron. Soc. Japan 46, 123.
Tomimatsu, A., Takahashi, M., 2003. Astrophys. J. 592, 321.
Tóth, G., Jia, X., Markidis, S., et al., 2016. J. Geophys. Res. (Space Phys.) 121, 1273.
Tzeferacos, P., Ferrari, A., Mignone, A., et al., 2009. Mon. Not. R. Astron. Soc. 1371.
Tzeferacos, P., Ferrari, A., Mignone, A., et al., 2013. Mon. Not. R. Astron. Soc. 428, 3151.
Uchida, Y., Shibata, K., 1985. Publ. Astron. Soc. Japan 37, 515.
Ustyugova, G.V., Koldoba, A.V., Romanova, M.M., Chechetkin, V.M., Lovelace, R.V.E., 1995. Astrophys. J. Lett. 439, L39.
Vaidya, B., Mignone, A., Bodo, G., Rossi, P., Massaglia, S., 2018. Astrophys. J. 865, 144.
Vernaleo, J.C., Reynolds, C.S., 2006. Astrophys. J. 645, 83.
Vernaleo, J.C., Reynolds, C.S., 2007. Astrophys. J. 671, 171.
Vlahakis, N., Königl, A., 2003. Astrophys. J. 596, 1080.
Vourellis, C., Fendt, C., Qian, Q., Noble, S., 2019, arXiv e-prints.
Wagner, A.Y., Bicknell, G.V., 2011. Astrophys. J. 728, 29.
Wagner, A.Y., Bicknell, G.V., Umemura, M., 2012. Astrophys. J. 757, 136.

Wagner, A.Y., Bicknell, G.V., Umemura, M., Sutherland, R.S., Silk, J., 2016. Astronom. Nachr. 337, 167.
Wald, R.M., 1974. Phys. Rev. D 10, 1680.
Waldrop, M.M., 2016. Nature 530 (7589), 144.
Walg, S., Achterberg, A., Markoff, S., Keppens, R., Porth, O., 2013, arXiv e-prints.
Walker, R.C., Hardee, P.E., Davies, F.B., Ly, C., Junor, W., 2018. Astrophys. J. 855, 128.
Weinberger, R., Ehlert, K., Pfrommer, C., Pakmor, R., Springel, V., 2017. Mon. Not. R. Astron. Soc. 470, 4530.
Xia, C., Teunissen, J., El Mellah, I., Chané, E., Keppens, R., 2018. Astrophys. J. Suppl. 234, 30.
Yokosawa, M., Ikeuchi, S., Sakashita, S., 1982. Publ. Astron. Soc. Japan 34, 461.
Zanni, C., Ferrari, A., Rosner, R., Bodo, G., Massaglia, S., 2007. Astron. Astrophys. 469, 811.
Zanni, C., Murante, G., Bodo, G., et al., 2005. Astron. Astrophys. 429, 399.
Zdziarski, A.A., Bottcher, M., 2015. Mon. Not. R. Astron. Soc. 450, L21.

Dr. Oliver Porth is assistant professor in computational astrophysical fluid dynamics at the Anton Pannekoek Institute for Astronomy / Amsterdam. After completing his Ph.D. on formation and evolution of relativistic jets with Dr. Christian Fendt at Max Planck Institute for Astronomy / Heidelberg (2011), he has taken on postdoctoral positions at Leeds/UK (with Prof. Serguei Komissarov), Leuven/Belgium (with Prof. Rony Keppens) and Frankfurt/Germany (with Prof. Luciano Rezzolla).

Dr. Porth has worked on a variety of subjects including solar physics, general relativistic accretion, jet formation- and stability and dynamics of pulsar wind nebulae. He has been maintainer and lead developer of community codes for astrophysical fluid dynamics and has led community wide code comparison efforts. Oliver Porth is part of the EventHorizonTelescope collaboration which was awarded the Breakthrough Price 2020 for constructing the first image of a black hole shadow.